TAMPEREEN TEKNILLINEN YLIOPISTO
TAMPERE UNIVERSITY OF TECHNOLOGY

HERTTA KARJALAINEN

COMBINING DIRECTED SELF-ASSEMBLY OF BLOCK COPOLYMERS WITH SOFT LITHOGRAPHY

Master of Science Thesis

Examiners:
Associate Professor Tapio Niemi,
Professor Nikolai V. Tkachenko
Examiners and topic approved by the Faculty Council of the Faculty of Natural Sciences on 4th of June 2014.

ABSTRACT

TAMPERE UNIVERSITY OF TECHNOLOGY
Master's Degree Programme in Science and Engineering
KARJALAINEN, HERTTA: Combining directed self-assembly of block copolymers with soft lithography
Master of Science Thesis, 69 pages, 3 Appendix pages
August 2014
Major: Chemistry
Examiners: Associate Professor Tapio Niemi, Professor Nikolai V. Tkachenko
Keywords: directed self-assembly, block copolymer lithography, soft lithography, microcontact printing, electron-beam lithography, nanoimprint lithography

Block copolymers (BCPs) are macromolecules consisting of two or more polymer blocks covalently joined together. These blocks may be thermodynamically incompatible, in which case the repulsive forces between the blocks initiate the formation of ordered structures at the molecular scale in dimensions of 5 – 50 nm. In thin films of block copolymers this phase separation behavior leads to nanoscale patterns of lamellae, cylinders or spheres depending on the composition and molecular weight of the block copolymer. These patterns can be guided by lithographically predefined structures that can be either topographic relief structures or chemically differentiated surface regions.

One application of BCPs in microfabrication is to combine block copolymer self-assembly with soft lithographic methods by using a block copolymer template as a master to fabricate an elastomeric stamp that can be used to transfer nanoscale patterns onto substrates. This stamp would have a high resolution pattern in dimensions unachievable by traditional lithographic methods that have commonly been used in stamp fabrication for soft lithography. Microcontact printing is one of the soft lithographic techniques in which the stamp is used to transfer monolayers of molecules onto a substrate. Using a stamp with nanoscale patterns to microcontact print a self-assembled monolayer (SAM) opens interesting prospects for arranging nanoparticles, such as quantum dots, in ordered manner on top of this SAM.

In this Thesis polystyrene-*block*-polymethyl metacrylate (PS-*b*-PMMA) block copolymer was used to fabricate PMMA cylinders in PS matrix ordered perpendicular to the supporting silicon substrates. Nanohole patterns of ~25 nm diameter were obtained after selective etching of the PMMA. It was found, that adding a thin silica layer on top of silicon substrates enhanced the quality of BCP assembly remarkably. Directed assembly of block copolymer domains on topographically pre-patterned substrates with various pattern shapes and dimensions was investigated. Nearly defect free assembly of PMMA cylinders in topographically defined trench patterns was obtained but the assembly in smaller square patterns was still found inadequate. Different dry etching methods for the BCP pattern transfer into the underlying substrates were tested and, consequently, the etching with CHF_3/O_2 plasmas was concluded to be the best etching recipe. The masters obtained were used to fabricate elastomeric h-PDMS stamps for microcontact printing. It was noted that the height of the patterns in the stamps is too low resulting from either too low etching of the masters or poor adjustment of the stamp material to the pattern. When investigating the microcontact printing with (3-Mercaptopropyl)trimethoxysilane (MPTMS) alkoxythiolate, the attachment of the monolayer with unpatterned stamp was confirmed by fluorescence lifetime microscopy but the stamping with patterned stamps still has to be developed further.

TIIVISTELMÄ

TAMPEREEN TEKNILLINEN YLIOPISTO
Teknis-luonnontieteellinen koulutusohjelma
KARJALAINEN, HERTTA: Lohkokopolymeerien ohjatun itsejärjestäytymisen hyödyntäminen pehmeässä litografiassa
Diplomityö, 69 sivua, 3 liitesivua
Elokuu 2014
Pääaine: Kemia
Tarkastajat: Associate Professor Tapio Niemi, Professori Nikolai V. Tkachenko
Avainsanat: ohjattu itsejärjestäytyminen, lohkokopolymeerilitografia, pehmeä litografia, mikrokontaktipaino, elektronisuihkulitografia, nanopainolitografia

Lohkokopolymeerit ovat makromolekyylejä, jotka koostuvat kahdesta tai useammasta kovalenttisesti toisiinsa sitoutuneesta polymeerilohkosta. Nämä lohkot voivat olla termodynamisesti yhteensopimattomia, missä tapauksessa Lohkojen väliset hylkimisvoimat aiheuttavat sen, että lohkot erottuvat spontaanisti toisistaan ja muodostavat järjestäytyneitä rakenteita, joiden mittasuhteet ovat molekyylin kokoluokkaa (5 – 50 nm). Ohuissa lohkokopolymeerikelmuissa tämä erottumiskäyttäytyminen johtaa nanokokoisten lamelli-, sylinteri- tai pallokuvioiden muodostumiseen. Muodostuvan kuvion rakenteen ja kokoluokan määräävät lohkokopolymeerin koostumus ja molekyylipaino. Näiden nanokuvioiden muodostumista voidaan lisäksi ohjata litografisilla esikuvioinneilla, jotka voivat olla joko topografisia kohokuviointeja tai kemiallisesti erilaistettuja pinta-alueita.

Eräs tapa hyödyntää lohkokopolymeerejä mikrokuvioinnissa on lohkokopolymeerien itsejärjestäytymisen ja pehmeiden lithografiamenetelmien yhdistäminen siten, että lohkokopolymeerikuviosta valmistetaan aihio, jota käyttäen puolestaan voidaan valmistaa elastomeerinen leimasin nanomeeristen kuvioiden siirtämiseen eri substraateille. Tällä tavoin valmistettuun leimasimeen saataisiin korkearesoluutioinen nanokuvio, jonka mittasuhteita ei voida saavuttaa perinteisillä litografiamenetelmillä. Mikrokontaktipaino on menetelmä, jossa leimasimen avulla pyritään siirtämään molekyylimonokerroksia substraatille. Painamalla mikrokontaktipainomenetelmällä itsejärjestäytyviä molekyylimonokerroksia käyttäen leimasinta, jonka kuviot ovat nanomittakaavassa, on mahdollista saavuttaa kuvioitu molekyylikerros, jonka päälle voidaan jälkeenpäin sitouttaa nanopartikkeleja, kuten kvanttipisteitä, hyvin järjestäytyneellä tavalla.

Tässä diplomityössä käytettiin polystyreeni-*b*-polymetyylimetakrylaatti (PS-*b*-PMMA) lohkokopolymeeriä, jonka avulla kuvioitiin piisubstraateille pintaa vasten kohtisuorassa olevia PMMA sylinterejä. Nanoreikäkuvio saatiin aikaiseksi, kun PMMA lohkot etsattiin selektiivisesti pois. Tutkimuksissa huomattiin, että ohuen SiO_2-kerroksen lisääminen substraatin pinnalle paransi kuvioiden järjestäytymistä huomattavasti. Lohkokopolymeerien ohjattua järjestäytymistä topografisesti kuvioitujen substraattien päälle tutkittiin erimuotoisilla ja -kokoisilla esikuvioinneilla ja saavutettiin lähes virheetön sylintereiden järjestäytyminen urakuvion pohjalle. Työssä tutkittiin myös erilaisia kuivaetsausreseptejä lohkokopolymeerikuvion siirtämiseksi alla olevaan substraattiin. Näistä CHF_3/O_2 etsaus todettiin tehokkaimmaksi. Etsaamalla valmistettuja aihioita käytettiin leimasimien valmistamiseen h-PDMS elastomeeristä, mutta huomattiin, että leimasimen kuvioiden korkeus on liian matala onnistunutta painoprosessia varten. Mikrokontaktipainoa kokeiltiin painamalla monokerroksia MPTMS alkoksisilaania substraateille sekä tasaisella, että kuvioidulla leimasimella. Monokerroksen sitoutuminen substraattiin vahvistettiin fluoresenssimikroskopian avulla, mutta kuvion siirtymistä kuvioidusta leimasimesta substraattiin ei havaittu.

PREFACE

This Thesis was conducted at Optoelectronics Research Centre (ORC) located in Tampere University of Technology. I would like to express my gratitude to Pekka Savolainen, the leader of ORC, for the opportunity to work in the great scientific environment there.

I would also like to thank my supervisors, Associate Professor Tapio Niemi from ORC and Professor Nikolai V. Tkachenko from the department of Chemistry and Bioengineering. The greatest acknowledgement for this Thesis goes without a doubt to Professor Tapio Niemi who has been guiding me throughout the time I have been working at ORC, and who first introduced me to nanoscience and the fascinating world of block copolymers and from whom I have learned so much about micro- and nanofabrication during my time at ORC.

Great thanks also go to all my fellow coworkers at ORC, who have taught me everything I now know about working in the cleanroom and using all the complex equipment there and who have also been great, fun company during the lunch and coffee breaks. M.Sc. Kirsi Virkki from the Department of Chemistry and Bioengineering has been a huge help when conducting the fluorescence lifetime microscopic measurements and I would like to express my gratitude for that.

Finally, I would like to thank my family, especially my mother Tiina and my sister Veera for all the love, support and belief I have received from you during my years of studying. My lovely friends both from TUT and the “old” ones from high school years have been the ones that have been able to get my mind off the science from time to time. Thank you guys for that! However, the deepest gratitude I want to express to my dear boyfriend Aku, who has been the one having to listen the constant talk about the progress of the Thesis, who has supported me during this whole process and who just makes each of my days (even the worst ones) always so much better. Thank You!

Tampere, 20th of August 2014.

Hertta Karjalainen

Contents

LIST OF SYMBOLS AND ABBREVIATIONS

T_g	glass transition temperature
T_m	melting point
$\bar{M}_n$	number-average molecular weight
$\bar{M}_w$	mass-average molecular weight
W_i	weight of polymer fraction i
PDI	polydispersity index
BCP	block copolymer
N	the degree of polymerization
f	the block copolymer composition
ΔG_{mix}	the free energy of mixing
k_b	Boltzmann's constant
T	temperature
χ	Flory-Huggins interaction parameter
Z	number of nearest-neighbor monomers to a copolymer configuration cell
ε	interaction energy
T_{ODT}	order-to-disorder transition temperature
t	the thickness of a block copolymer thin film
L_0	the domain period in a block copolymer
PS-*b*-PMMA	polystyrene-*block*-polymethyl metacrylate block copolymer
SAM	self-assembled monolayer
RIE	reactive ion etching
DSA	directed self-assembly
PS-*r*-PMMA	polystyrene-*co*-polymethyl metacrylate random copolymer
EBL	electron beam lithography
SEM	scanning electron microscopy
L_s	lattice pitch of an electron beam prepattern
μCP	microcontact printing
NIL	nanoimprint lithography
QD	quantum dot
PECVD	plasma-enhanced chemical vapor deposition
FDTS	perfluorodecyltrichlorosilane, antiadhesion chemical
MPTMS	(3-mercaptopropyl)trimethoxysilane

1 INTRODUCTION

Microfabrication, the generation of small structures, is an essential part of modern science and technology. It supports information technology and has an influence on society through its role in microelectronics and optoelectronics. The progress of microfabrication rests mainly on the ability to create precisely ordered micro- and even nanoscale structures in increasingly small dimensions. For decades, the predominant nanopatterning method has been photolithography that utilizes light to write patterns onto photosensitive materials called photoresists. However, as the sizes of device features become ever smaller, conventional lithographic processes become increasingly difficult and more expensive, especially at a minimum feature size of less than 45 nm. This has led the scientists to look for other alternatives for nanoscale pattern production. [1], [2]

Block copolymers are a class of self-assembling materials that offer an attractive alternative patterning technology because they segregate to form self-assembled nanopatterns on nanometer length scales. [3] Diblock copolymers that consist of two polymer chains covalently linked together are used for lithography applications. During the self-assembly process, diblock copolymer thin films with spherical, cylindrical or lamellar morphologies of different scales may be created by adjusting the composition and molecular weight of the block copolymer. Moreover, these domains can be guided into ordered structures by topographical relief patterns or chemical modification of the underlying surface. During the past decade, block copolymer thin films have been the subject of numerous scientific papers in which they have been demonstrated to be able to fabricate quantum dots [4], magnetic storage media [5], nanowires [6] and nanopores [7] and act as templates for nanoimprint lithography (NIL) [8] to mention some of the applications.

Soft lithography developed by *Whitesides et al*. is another technology for overcoming the problems related to microfabrication by photolithography. The soft lithographic methods all share the common feature: they use a patterned elastomer as the mask, stamp or mold to create micropatterns and utilize flexible organic molecules and materials rather than the rigid inorganic materials commonly used in microfabrication. Microcontact printing (μCP) and nanoimprint lithography (NIL) are two lithography methods that both use an elastomeric stamp for pattern creation. In microcontact printing the elastomeric stamp is used to transfer molecules of the “ink” to the surface of the substrate by contact. The ink is usually a chemical that is able to form self-assembled monolayers (SAMs) on the substrate, e.g. alkanethiolate or siloxane monolayers. These SAMs can then be used as deposition sites of other molecules or as etch masks to transfer the pattern into the substrate. [9], [10] Again, in nanoimprint lithography, the elas-

tomeric stamp is used to convert the pattern in the stamp to a thin layer of resist on a substrate. The stamp is pressed against this resist which is then cured either thermally or with UV-light to transfer the stamp pattern into the resist, which can then act as an etch mask and the pattern can be etched to the substrate. [11]

The masters that are used to fabricate the elastomeric stamps can be made by optical lithography in which case one of the resolution limits is the wavelength of light and it becomes a problem at nanoscale patterning. Alternatively, the masters can be made by direct write methods such as electron beam lithography, by which sub-10 nm patterns can be achieved but, on the other hand, these direct write methods are very expensive and time consuming. The utilization of block copolymer lithography to easily fabricate a master with large areas of nanopatterns and soft lithography to efficiently produce multiple copies of this master pattern is an intriguing idea worth developing further. Moreover, with an elastomeric stamp in sub-30 nm pattern scale, microcontact printing of alkanethiolate SAMs in dimensions suitable for attachment of colloidal quantum dots (diameter 6-10 nm) could be possible. The ordered arrangement of quantum dots into desired patterns is desirable, for example, in developing quantum dot cellular automata (QCA) for future nanoelectronic devices and logic circuits [12]. The motivation for this Thesis is to study the methods to combine these three subjects, block copolymer lithography for master fabrication, soft lithographic methods for forming an ordered SAM and finally quantum dots to be linked to the SAM deposited on the substrate surface.

Block copolymer lithography is a new area of research in Optoelectronics Research Centre (ORC) where this Thesis has been conducted and the first goal for the Thesis is to establish a functional process scheme for block copolymer lithography on non-patterned and patterned surfaces using cylinder forming polystyrene-*block*-polymethyl metacrylate (PS-*b*-PMMA) block copolymer. These block copolymer templates are then utilized as masters to fabricate an elastomeric stamp for microcontact printing, replicating the relief pattern of the self-assembled block copolymer structure. The application of MPTMS alkanethiolate ((3-Mercaptopropyl)trimethoxysilane) monolayer on a substrate by microcontact printing is also studied by fluorescence lifetime microscopy. The methods used to study the block copolymer templates are scanning electron microscopy and atomic force microscopy.

2 POLYMERS AND BLOCK COPOLYMERS

Polymers are macromolecules consisting of large numbers of repeating units called monomers that are joined together by covalent bonds. Polymer molecules have large molecular weights of several thousand g/mol or even more. Polymerization can take place by a self-reaction of one monomer (e.g. polystyrene) or from a mutual reaction of two or more monomers. Polymers can be classified in several different means, one of which is classification by polymer structure. A polymer structure can be described as linear, branched, cross-linked, ladder-shaped, star-shaped, comb-shaped or dendritic as shown in Figure 2.1.

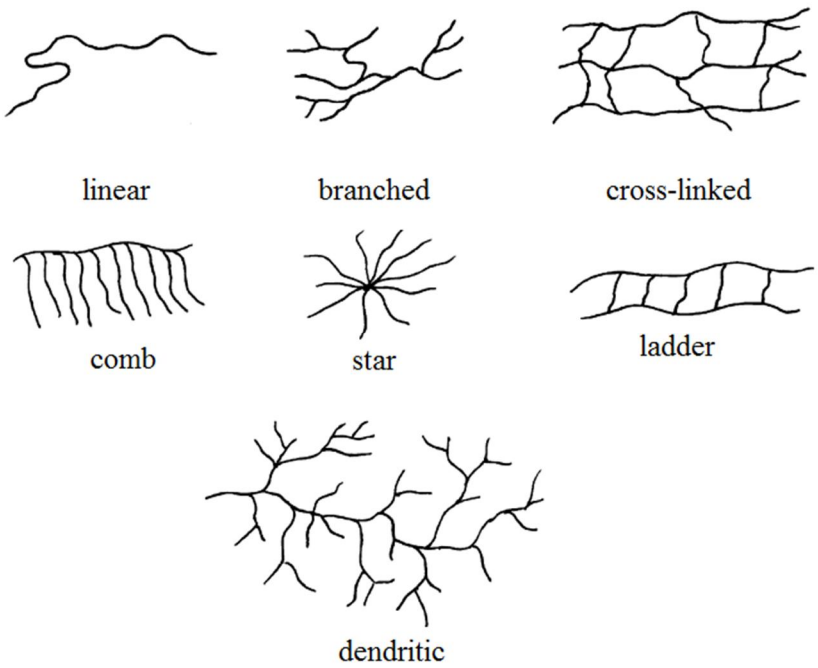

Figure 2.1. *Schematic representation of different polymer structure types.*

In addition, polymers can be classified by the origin of the polymer (natural or synthetic), by functional groups present in the repeating unit (polyesters, polyamides etc.), by polymerization mechanism (condensation vs. addition, chain-wise vs. step-wise polymerization), by polymerization technique (e.g. bulk, solution or emulsion polymerization), by thermal behavior (thermoplastics and thermosets) or by the end use of the polymer (e.g. diene polymers for rubber industry and acrylics for coating). [13], [14]

2.1 Polymer morphologies

Polymer morphology describes the arrangement and microscale ordering of polymer chains in space. There are two common polymer morphologies: crystalline and amorphous. Amorphous sate is produced by the lack of order in the arrangement in polymer chains whereas polymers chains with very regular structures tend to be more crystalline. The synthetic polymers, however, cannot be entirely crystalline but always have also an amorphous portion and as of that are called semicrystalline polymers. The degree of crystallinity is the fraction of the total polymer in the crystalline regions and it may vary from a few percentages to about 90 % [13]. Crystallinity makes a polymer strong but also brittle and the amorphous regions give a polymer more ability to bend without breaking. Polymer structure and intermolecular forces within the polymer are the factors influencing the morphology of a polymer. For example, branched polymers tend to be more amorphous than linear ones as the latter can pack easily into defined structures. Intermolecular bonds like hydrogen bonds also induce crystallinity.

Glass transition temperature, T_g, marks the transition point where the polymer changes from the hard and brittle glassy state to the soft and flexible rubbery state. All polymers that have even a small amorphous portion (that is basically all polymers) have a glass transition temperature. Hard plastics like polystyrene are used below their T_g, in their glassy state, whereas elastomers like polyisoprene (natural rubber) are used above their T_g, in the rubbery state. On the other hand, only crystalline polymers have melting temperatures, T_m, at which the polymer chains fall out of their crystalline structure and become a disordered liquid. [13] A diagram of the thermal transitions of crystalline and amorphous polymers is shown in Figure 2.2.

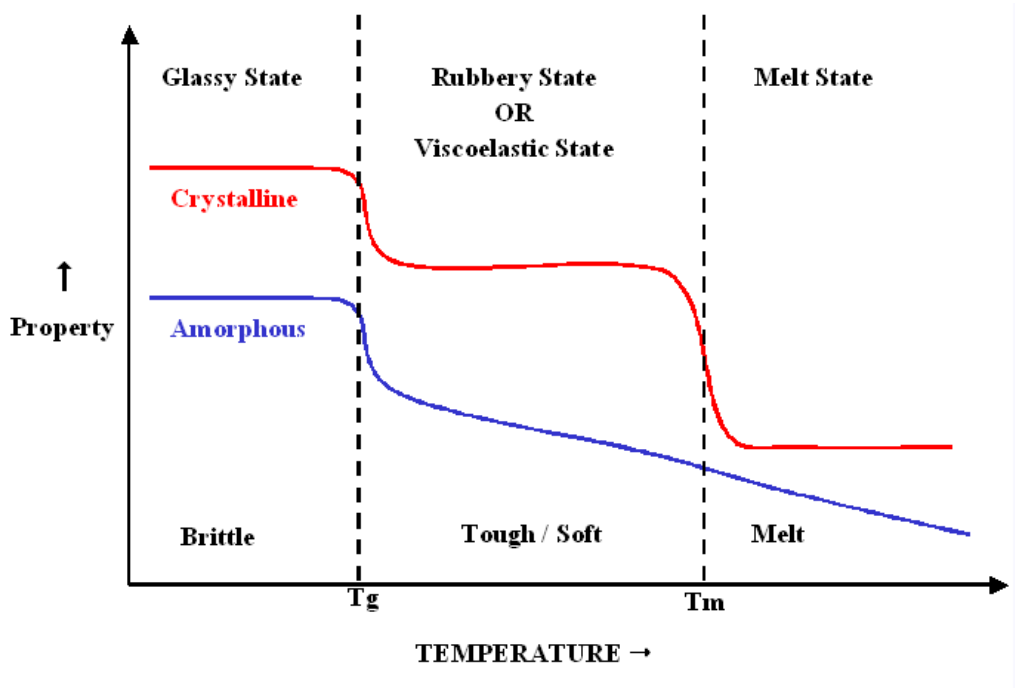

Figure 2.2. *Thermal transitions in polymers. The transitions from glassy state to rubbery and melt state are illustrated as the function of growing temperature. [15]*

In Figure 2.2 the red line illustrates the behavior of crystalline polymer and blue line that of an amorphous polymer. What should be noted is that while the red line has visible slopes at both glass transition and melting temperatures, the distinct transition in soft-melt region is lacking from the amorphous, blue line. Amorphous polymers do not have a certain melting point but the transition from the rubbery state to the disordered melt happens gradually.

2.2 Molecular weights of polymers

Molecular weight is an important factor characterizing the polymer as it is related directly to polymer's physical properties. Except for some natural occurring polymers, all polymers consist of molecules of different molecular weights and therefore the molecular weight of polymers is expressed in terms of an average value. The two most important average molecular weights are number-average molecular weight and mass-average molecular weight.

Number-average molecular weight ($\bar{M}_n$) describes the total weight of all the polymer molecules in the sample divided by the total number of polymer molecules in the sample:

$$\bar{M}_n = \frac{W_i}{\sum_{i=1}^{\infty} N_i} = \frac{\sum_{i=1}^{\infty} N_i M_i}{\sum_{i=1}^{\infty} N_i} \tag{2.1}$$

In the equation above, W is the total weight of the polymer and N_i is the number of polymer molecules with weight M_i.

Mass-average molecular weight ($\bar{M}_w$) is based on the fact that a larger molecule accounts for more of the total mass of the polymer sample than the smaller molecules:

$$\bar{M}_w = \frac{\sum_{i=1}^{\infty} W_i M_i}{\sum_{i=1}^{\infty} W_i} = \frac{\sum_{i=1}^{\infty} N_i M_i^2}{\sum_{i=1}^{\infty} N_i M_i} \tag{2.2}$$

In this equation, w_i is the weight of polymer fraction i. For all the synthetic polymers, $\bar{M}_w$ is greater than $\bar{M}_n$. Besides $\bar{M}_n$ and $\bar{M}_w$, there are also two other ways of expressing the average molecular weight of a polymer sample, which are viscosity-average molecular weight ($\bar{M}_v$) based on sedimentation behavior of the polymer and Z-average molecular weight ($\bar{M}_z$) that derives from the flow behavior of the polymer. [13], [14]

As there can be a number of chains of different sizes in a polymer sample, the average molecular weight is not enough to evaluate the polymer properties but the dispersion pattern must be known as well. Polymers are polydispersed systems that consist of molecules, each of which have a different molecular weight in contrast to monodispersed systems in which all the molecules are exactly the same. The polydispersity index (PDI) is an important parameter that is a measure of molecular mass distribution in

a given polymer sample. PDI is defined as the quotient of mass-average molecular weight, eq. (2.2), and number-average molecular weight, eq. (2.1):

$$\boldsymbol{PDI = \frac{\bar{M}_w}{\bar{M}_n}} \tag{2.3}$$

The value of PDI is always more than one, but as the polymer chains approach uniform chain length, the PDI approaches unity. The polydispersity can be expressed by a molecular weight distribution curve by plotting the number fraction (n_i) of molecules having the same particular molecular weight (M_i) against that corresponding molecular weight. Distribution curves for two polymer samples having the same number-average molecular weight but completely different PDIs are shown in Figure 2.3.

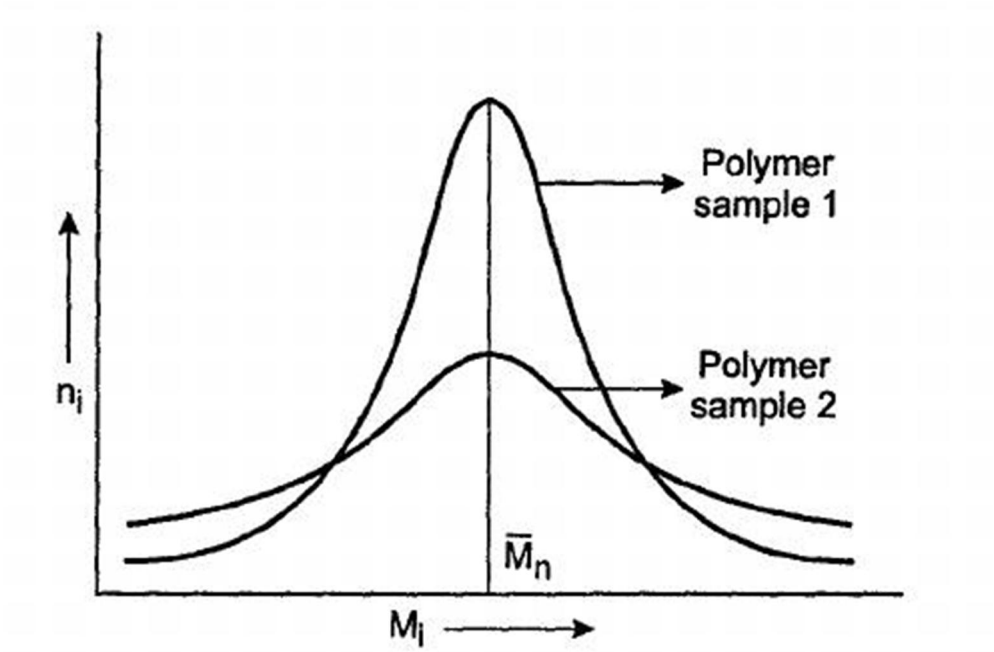

Figure 2.3. *Polydispersities of two polymer samples having the same number average molecular weight. The PDI of sample 1 is considerably narrower that the PDI of sample 2. [14]*

The lower the PDI, the more uniform the polymer sample is in terms of molecular weight. Most of the synthetic polymers have PDIs in the range of 10 – 20, but by utilizing the living polymerization reaction polydispersities as low as 1.06 can be achieved. The PDI in some naturally occurring biological polymers can be very close or even equal to 1. [13], [14], [16]

2.3 Block copolymers

Polymers consisting of only one monomer unit are called homopolymers, whereas copolymers are built of two or more different repeating units. The exact sequence of monomer units along the block copolymer chain can vary a lot depending on the relative reactivites of each monomer during the polymerization process. According to monomer unit arrangement, copolymers can be divided into random copolymers, alternating copolymers, block copolymers (BCPs) and graft copolymers. [13] These different types are represented in Figure 2.4.

Figure 2.4. *Copolymer structures of block copolymers consisting of repeating units A and B.*

In alternating copolymer, each monomer of one type is joined to a monomer of a second type and thus it is an ordered arrangement of two alternating repeating units along the polymer chain. Random copolymer is a complete opposite of alternating copolymer as the orientation of the units is totally random and unpredictable. Graft copolymers consist of sequences of one monomer grafted onto a backbone of another monomer type. As for block copolymers, they contain a block of one monomer followed by a block of another. The lengths of the blocks as well as the number of them can vary depending on the polymerization conditions. [13]

Here the block copolymers are covered in more detail, as they are the main topic of this Thesis. Different block copolymer architectures include the linear AB diblock, ABA triblocks and $(AB)_n$ multiblocks that are formed by joining two monomer types A and B together. Use of three or more monomer types leads to the formation of ABC triblock copolymers or multicomponent architectures. The strucuture of the block copolymers can also be linear or branched. [3] Some of the typical architectures are schematically depicted in Figure 2.5.

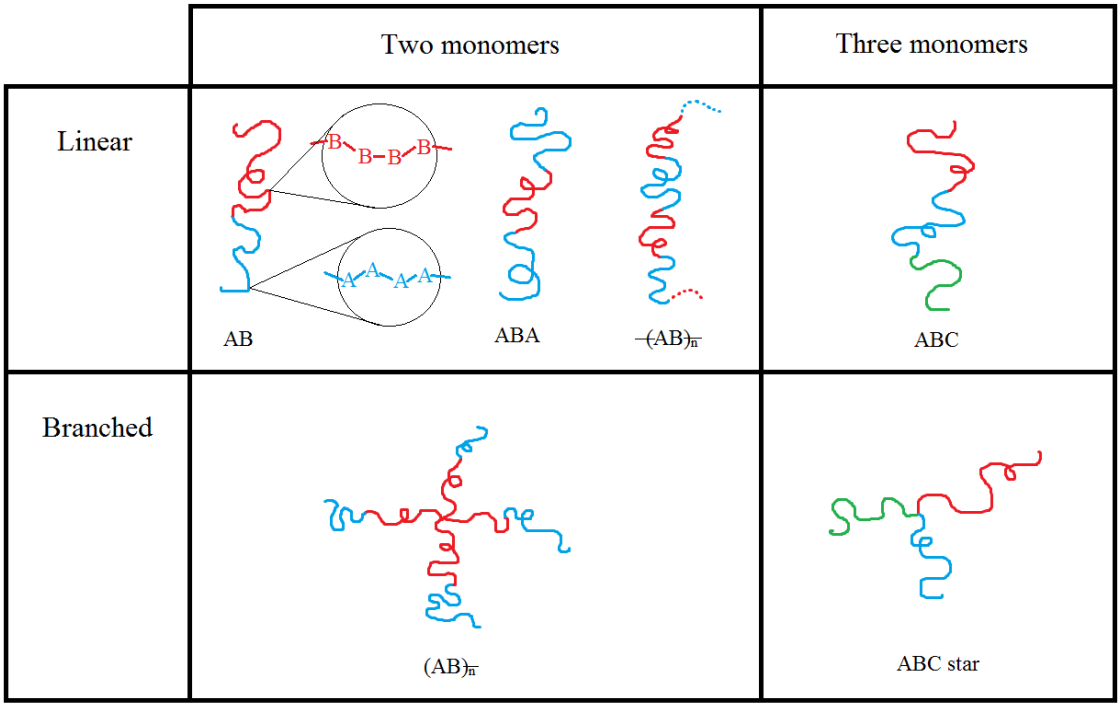

Figure 2.5. *Different molecular architectures of block copolymers classified according to number of monomer types (two or three) and sequencing (linear or branched). Each colored strand represents one polymer block composed of a linear sequence of same type monomers A, B or C (blue, red and green respectively).*

Block copolymers are interesting for microfabrication applications due to their unique characteristics to phase separate into nanoscale patterns. The two blocks joined together in a block copolymer may be thermodynamically incompatible. Because of the thermodynamical incompatibilities and the intermolecular repulsive forces, the blends of polymers tend to phase separate. However, in the case of block copolymers the two polymer blocks are unable to phase separate at macroscopic length scales as they are joined by covalent bonds and instead they spontaneously form ordered structures at the molecular scale with dimensions of 5 - 50 nm. The size and shape of the domains depends on the molecular weight and composition of the copolymer as explained in later chapters. [17]

2.3.1 Phase separation

The applications of block copolymers rely on their unique characteristic to self-assemble in the molten and solid states. This self-assembly process produces periodic composition patterns that can exhibit considerable complexity. These patterns in block copolymers are referred to as microphases and the term microphase separation is used to describe the formation of patterns in block copolymer melts. Due to the connectivity of the blocks, the dimensions of the domains are of molecular scale and, as such, nanoscopic.

Microphase separation is driven by chemical incompatibilities between the different blocks in block copolymers. The two blocks are mutually repellant and tend to separate into well-ordered microdomains. If the blocks were not connected to each other by covalent bonds, repulsive forces would lead to macrophase separation, which means segregation into regions of each homopolymer. However, in block copolymers the different blocks are bound to each other and because of that they cannot macrophase separate but instead minimize the repulsive energy by microphase separating into microdomains. [3], [18]

The microphase separation of block copolymers can be described thermodynamically using the Flory-Huggins theory, which describes the energetics and equilibrium behavior of a binary mixture such as a polymer and solvent or a blend of two linear homopolymers [19]–[21]. Here the theory is applied to qualitatively describe the microphase separated structure of diblock copolymers.

There are two parameters that influence the molecular structure of the block copolymer. These parameters are the overall degree of polymerization N, which is the total number of monomers per macromolecule and the composition $f_A = N_A/N$, where N_A is the number of A monomers per molecule. For a symmetric AB diblock copolymer $f_A = f_B = 0{,}5$. In an incompressible, two-component system of A and B, in which the volume fraction of A is f_A and the volume fraction of B is f_B and the number of A and B molecules are N_A and N_B respectively, the free energy of mixing, ΔG_{mix}, is given by

$$\frac{\Delta G_{mix}}{k_B T} = \frac{f_A}{N_A}\ln(f_A) + \frac{f_B}{N_B}\ln(f_B) + \chi f_A f_B \tag{2.4}$$

In the equation above the free energy is represented in units of thermal energy, k_BT. On the right side of the equation, the first two terms are the combinatorial entropy of mixing of each component and the third term accounts for the energy interaction between the two components [22]. Term χ is the Flory-Huggins interaction parameter which quantifies the repulsion between the two components A and B:

$$\chi_{AB} = \frac{Z}{k_B T}\left[\varepsilon_{AB} - \frac{1}{2}(\varepsilon_{AA} + \varepsilon_{BB})\right] \tag{2.5}$$

In equation (2.5) Z is the number of nearest-neighbor monomers to a copolymer configuration cell, ε_{AB} is the interaction energy per monomer between A and B monomers while ε_{AA} and ε_{BB} are interaction energies for each component itself. Positive χ_{AB} indicates that the mixture will phase separate, while a negative or small positive value means that the two components are miscible. [3] In general, the Flory-Huggins interaction parameter can be estimated with the equation

$$\chi = \frac{a}{T} + b \tag{2.6}$$

where *a* and *b* are experimentally obtained constants for enthalpy and excess entropy, respectively, for a given composition of particular block copolymer. The parameters may depend on *f*, *N* and *T*. According to equation (2.6), χ can be controlled through temperature. [3], [22]

Microphase separation takes place at temperature below an order-disorder transition temperature T_{ODT}. At temperatures higher than T_{ODT} the polymers are in a disordered phase and polymer blocks are homogenously mixed. The strength of separation is proportional to the term χN. The location of the order-disorder transition for symmetric diblock copolymers is $\chi N = 10.5$ as obtained by mean-field estimation by Leibler et al. [23] This means that diblock copolymers of high molecular weight (high *N*) or with stronger repulsion between blocks (high χ) have values of $\chi N > 10.5$ and are predicted to microphase separate, whereas smaller copolymers with more compatible blocks ($\chi N < 10.5$) are predicted to show no microphase separation. What the term χN really describes is the strength of the repulsive interactions in the block copolymer. When these interactions are strong enough, microphase separation will take place. [3]

The configurations of microphase separated nanostrucutres alter according to the block copolymer composition *f*. Matsen and Schick examined the microphases of diblock copolymer melts using the self consistent mean-field theory (SCFT) and calculated a phase diagram for AB diblock copolymers (Figure 2.6) [24]. For χN values lower than 10.5 only a disordered melt is predicted. At larger values of χN above the order to disorder transition (ODT) curve five ordered microphase structures are found. Nearly symmetric diblock copolymers form a lamellar phase, while a hexagonally packed cylinder phase is stable for diblocks with intermediate levels of compositional asymmetry. As the compositional asymmetry increases, the spherical phase becomes dominant. A very narrow region of close-packed spheres separates the disordered and spherical phases. A complex gyroid phase takes place on narrow regions close to the ODT and between lamellar and cylindrical phases.

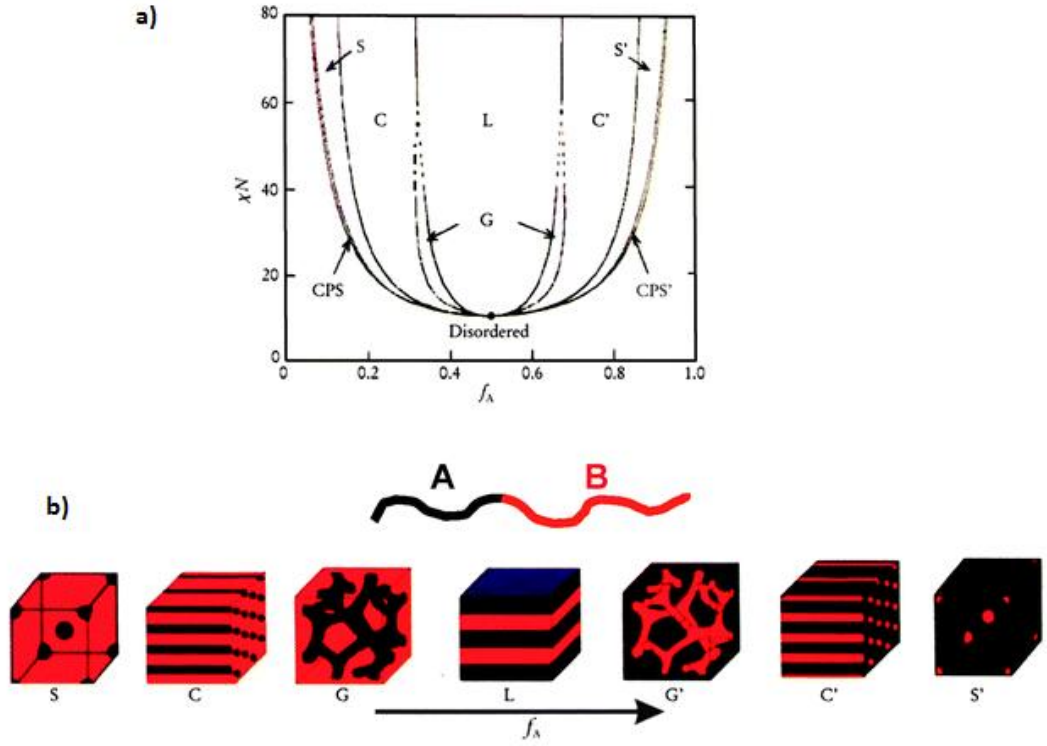

***Figure 2.6**. a) Phase diagram for diblock copolymers predicted by self consistent mean field theory includes five different morphologies: spherical (S), close packed spherical (CPS), cylindrical (C), gyroid (G) and lamellar (L) depending on the composition f and combination parameter χN. Below the ODT curve only disordered melt is predicted. [24] b) Equilibrium microdomain structures of a AB diblock copolymer as f_A is increased for fixed χN [3].*

Symmetrical ($f_A = f_B = 1/2$) or nearly symmetrical diblock copolymers arrange into lamellar morphologies. When $f_A < 1/2$ cylindrical phase forms as the smaller A blocks pack into the interiors of the cylinders (Figure 2.7). This allows the longer B blocks to reside on the convex side of the A-B interface reducing the elastic energy and is thus energetically favorable arrangement. When the compositional asymmetry increases more, the body centered cubic spherical phase (S) becomes dominant as the even smaller A blocks pack into the spheres. A very narrow region of close packed spheres (CPS) separates the disordered and spherical phases. Gyroid (G) phase is a narrow region of stability close to the ODT and between lamellar and cylindrical phases. Gyroid phase is a complex, bicontinious structure that is present in all soft condensed matter systems. [3], [24]

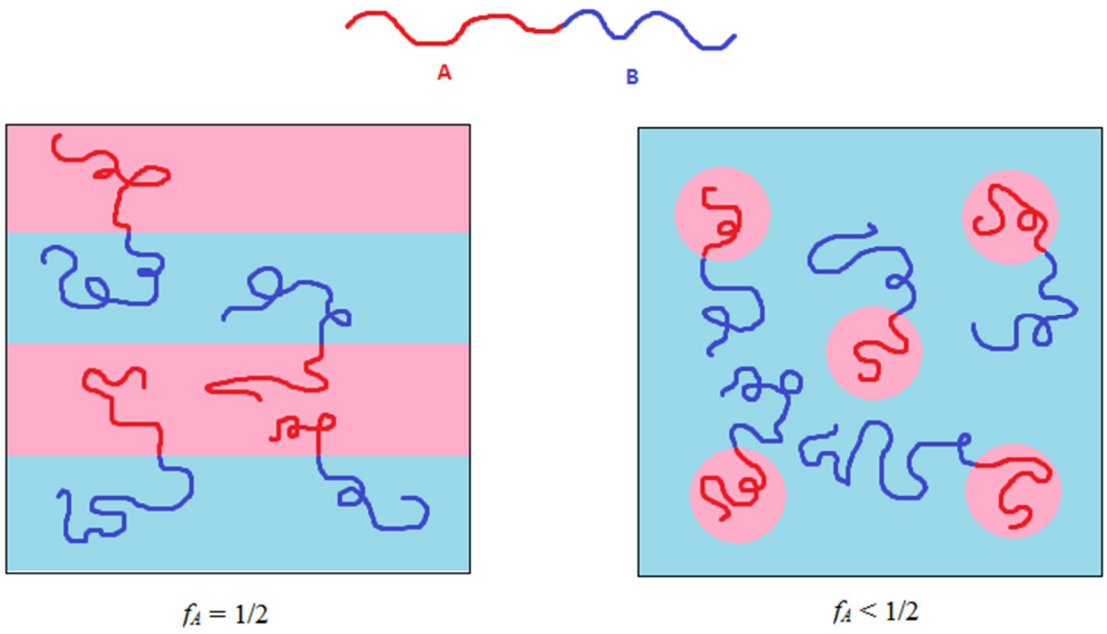

Figure 2.7. *The morphologies of AB diblock copolymers. The self assembly of nearly symmetrical compositions leads to lamellar morphology. Decreasing the volume fraction of one block (in this case block A) induces interfacial curvature resulting in nonlamellar morphology such as cylindrical or spherical. [3]*

The dimensions of nanodomains can be controlled by changing the molecular weight of the block copolymer. The smallest sizes are limited by the segregation term χN. Small molecular weight polymers have small degree of polymerization, N. If the molecular weight is small enough the term χN reaches the limit of phase separation (10.5) and the polymer exists only as disordered melt. On the other hand, the large size scale limit is set by the kinetics of ordering, which is really slow for higher molecular weight polymers. [25]

2.3.2 Block copolymer thin films

So far the discussion has concerned block copolymers in bulk. However, in block copolymer lithography applications, thin films with thicknesses of less than ten microdomain spacings are commonly used. In thin films, the microdomains tend to form with a particular orientation to the substrate surface as demonstrated in Figure 2.8. The surface perpendicular lamellae and surface parallel cylinders are of particular interest for nanowire patterning, whereas the surface perpendicular cylinders and spheres may be utilized for example in the patterning of hexagonal arrays for data storage. [22]

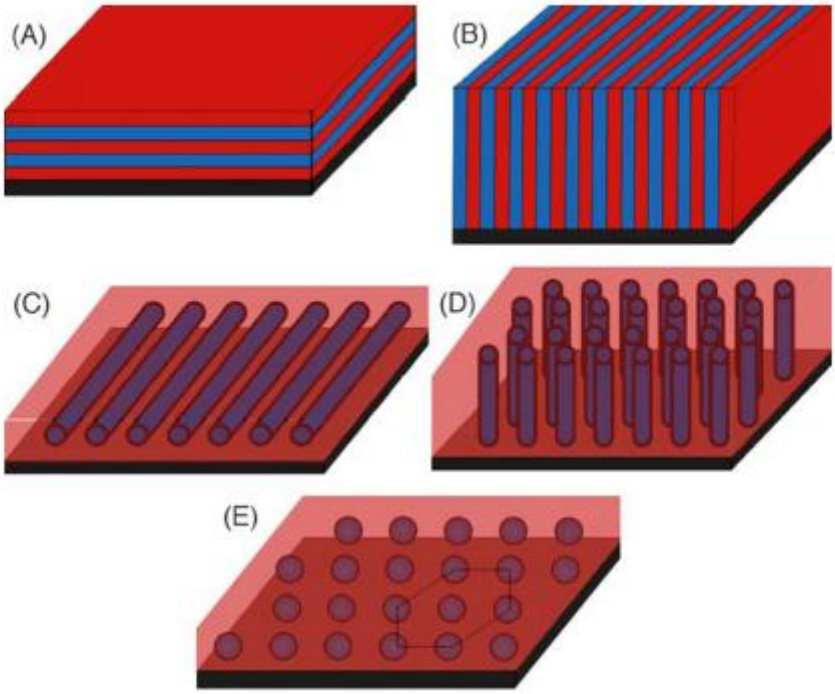

Figure 2.8. *Different block copolymer orientations in thin films. (A) Lamellae lying parallel to the substrate, (B) lamellae aligned perpendicular to the substrate, (C) parallel cylinders, (D) perpendicular cylinders and (E) spheres.[22]*

In thin films, the orientation and morphology of microdomains are influenced by the film thickness t relative to bulk state natural domain period L_0 and the interaction energetics at the air/polymer and polymer/substrate interfaces. For polymer blocks of different chemical composition, the interfacial energies are different, which leads to preferential wetting of each interface by selective blocks. For example polar poly(methyl metacrylate) (PMMA) domains in polystyrene-*block*-poly(methyl metacrylate) (PS-*b*-PMMA) block copolymers preferentially wet the hydrophilic native oxide layer of a silicon substrate whereas the nonpolar polystyrene (PS) block with lower surface energy assembles at the air interface. This leads to surface parallel microdomain orientation where symmetric PS-*b*-PMMA arranges into surface parallel layers of lamellae PMMA block lying at the substrate/polymer interface and PS block the topmost at the air/polymer interface. [26], [27] In the case of cylinder or sphere forming PS-*b*-PMMA where PMMA is the minority block the PMMA block wets the surface resulting in an extra half layer of film, the wetting layer. On top of the wetting layer lie the surface parallel PMMA cylinders or spheres in PS matrix. This behavior has been confirmed by *Harrison et al*. for poly(styrene)-*block*-poly(butadiene) (PS-*b*-PB, PS majority block) on PMMA-coated and native oxide silicon substrates. [28] Schematics of both lamellar and cylindrical thin film morphologies are presented in Figure 2.9.

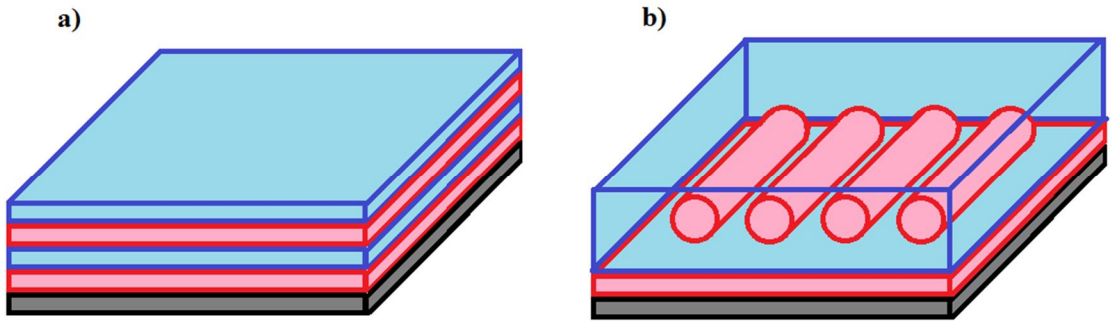

***Figure 2.9**. Nanodomain orientation in PS-b-PMMA on a silicon substrate. PMMA domains (red) preferentially wet the substrate and the PS domains (blue) the polymer/air interface. a) Lamellar morphology. b) Cylindrical morphology.*

The wetting behavior of PS-b-PMMA block copolymer is called asymmetric wetting, as one block wets the substrate/polymer interface and the other block wets the air/substrate interface. Symmetric wetting happens when one block is located on both the air surface as well as the substrate [29]

A consequence of the interfacial interactions is a quantization of film thickness, sometimes called terracing. In a diblock copolymer exhibiting symmetric wetting behavior, a film that is one molecular layer thick will be frustrated because block A cannot wet both the substrate and the free interface. As a result, the thinnest stable film will be two molecular layers thick with the B block constrained inside the film surrounded on top and bottom by A blocks. This thickness is referred to as L_0 (natural domain period) and only the film thicknesses $t = nL_0$ are allowed (n is an integer). Similarly, for the asymmetric-wetting diblocks $½L_0$ is the thinnest stable film and the quantization restriction $t = (n+ ½)L_0$ applies. [29], [30] Figure 2.13 displays these two wetting scenarios for lamellar phase, although analogous situation applies to other morphologies as well.

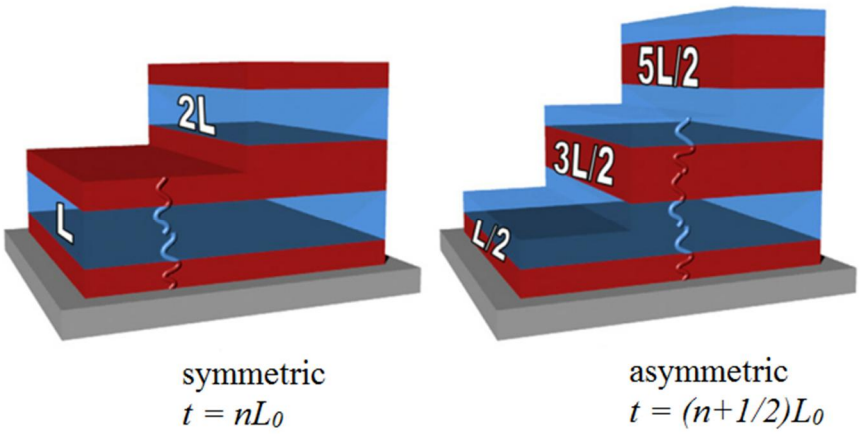

Figure 2.10. *Selective interfacial wetting in block copolymer thin films. [31]*

As a result of this quantization, a thin film coated at an incommensurate thickness will segregate into regions of quantized thickness upon annealing. This leads to the development of +1 and -1 layers, in which the defect structures are called islands and holes, respectively. *Smith et al*. investigated the formation of islands/holes for incommensurate film thicknesses as a function of molecular weight of the polymer and found out that close to the commensurability condition, the films appear featureless but with increasing film thickness the morphology progresses from islands to spinoidal island/hole structures to holes to featureless again at the next commensurate thickness. [32] Determination of the commensurability condition is more difficult for block copolymer microstructures more complex than lamellae, but the same principle of island and hole formation on preferential surfaces applies. [22]

Perpendicular alignment of lamellae and cylinders is often desirable for lithographic applications and can be achieved by several means. To generate perpendicular orientation, the interaction between each block and substrate should be similar. The most common approach to generate a neutral surface is to treat the substrate with a random copolymer brush layer that contains the same monomers as the block copolymer. [33] Random copolymers are usually end-functionalized with a hydroxyl group that is used to end-graft the random copolymer chains to the native oxide layer of the silicon substrate. For instance, a polystyrene-*ran*-poly(methyl metacrylate) (PS-*r*-PMMA) brush layer with an end-functional OH-group can be attached to the native silicon oxide layer of a silicon substrate. This random layer has similar affinity towards both PS and PMMA blocks in PS-*b*-PMMA block copolymers, which directs the microdomains into perpendicular orientation because neither of the blocks does not wet the surface alone but instead they both settle on the surface and thus the nanopatterns are formed upwards, perpendicular to the substrate instead of the patterns lying parallel to the substrate when one block wets the whole substrate.

Besides grafting the random copolymer chemically to the substrate, a neutral surface layer can also be obtained by using self-assembled monolayers (SAMs) [34],

[35] or by including thermal- or photo-crosslinkable groups into the random copolymer, which allows the formation of a neutral layer regardless of the surface chemistry of the underlying substrate [36] One method for surface neutralization is to use a ternary blend of end-functionalized homopolymers A and B and a low molecular weight A-*b*-B block copolymer. The block copolymer acts to homogenize the A/B homopolymer mixture (prevents macrophase separation of the homopolymer blend) before the homopolymers are grafted on the substrate via their functional groups. [37]

Although the most used, surface neutralization is not the only way to obtain surface perpendicular nanodomains. Other known methods are to use an electric field [38]–[40], magnetic field [41], solvent annealing [42] or directed assembly on chemically [43], [44] or topographically [45] nanopatterned surfaces.

2.3.2.1 General process steps for thin film preparation

A variety of different methods can be used for preparing thin films of block copolymers on substrates but the process described here is widely used and has been established as a the basic BCP thin film deposition method.

The solution of the copolymer is prepared in a good, volatile, organic solvent (usually the concentration is about 1 - 2 wt %) and spin coated onto the substrate. The spin coating is done at 1000 - 5000 rpm and the substrate is spun until the solvent is evaporated from the film. Silicon wafers are often used as the substrate due to their uniform flatness. The concentration of the solution, the molecular weight of the polymer, the volatility of the solvent and the spin speed are the factors that determine the film thickness. The desired thickness is usually about 30-50 nm. [46][47]

The deposition is usually followed by an annealing step to facilitate or accelerate microphase separation and microdomain formation in the BCP film. Annealing increases the mobility of the copolymer molecules, so the film can more rapidly reach its equilibrium structure. Annealing can be achieved thermally or with a solvent vapor treatment. In thermal annealing the sample is held at a temperature above the glass transition temperatures but below decomposition temperatures of the polymer blocks for a time sufficient to allow the formation of the equilibrium morphology. Thermal annealing can be carried out under vacuum or in an inert gas environment. Solvent annealing is achieved by holding the sample in a controlled atmosphere containing selected solvent vapors. The absorption of the vapor causes greater mobility within the film. The efficacy of the annealing depends on the selectivity of each block to the solvent and a variety of solvents or mixtures of solvents can be used.

For many applications, a three-dimensional relief image is the desired final nanostructure and for BCPs this calls for a means to selectively remove one (usually the minor) block. For PS-*b*-PMMA this can be done by a simple reactive ion etching (RIE) step with oxygen or a mixture of oxygen and argon or by treating the block copolymer film with UV irradiation which degrades the bonds within PMMA blocks and then removing PMMA domains by rinsing the sample repeatedly with acetic acid. [46]

2.4 Directed self-assembly of block copolymers

The most important quality of block copolymers is their ability to phase separate into nanodomains at the molecular scale. However, the orientation of these nanodomains is frequently not perfect. A lot of work has been done to control the self-assembly and orientation of the domains. Typically, lithographically predefined structures that can be either topographic relief structures or chemically modified surface regions are used to direct and control the placement. Directed self-assembly (DSA) has been demonstrated for a variety of microdomain morphologies with each targeted at specific potential application. Several common DSA methods for BCPs are reviewed in the next section.

2.4.1 Topographical prepatterning

Graphoepitaxy, which means utilizing a topographical surface relief structures to induce crystallographic orientation in thin films, is a widely used method for directed self-assembly of block copolymers. [48], [49] A variety of conventional lithographic methods, including interference lithography [50], [51] and electron beam lithography [52]–[54], can be used to fabricate the substrates with relative ease. After the lithography step block copolymer thin film is spin coated and annealed on top of the patterned substrate. The underlying topographical pattern then directs the formation of the nanopattern. The wetting properties of the surface pattern bottom and walls as well as the commensurability of the pattern and the block copolymer have to be carefully considered in order to achieve good ordering behavior. Trench patterns are one of the most used topographical patterning application and lamellar, cylindrical and spherical nanodomain orientations have all been guided with trench patterns. [49], [51], [52], [54]

The parameters that influence the degree of ordering in topographically directed self-assembly are the commensurability of the pattern with the block copolymer microdomain period L_0, the thickness of the block copolymer film or the depth of the pattern and the interaction of the polymer with the walls and bottom of the pattern. *Segalman et al*. investigated the graphoepitaxial patterning of spherical PS-*b*-P2VP block copolymers into patterns consisting of long trenches of alternating series of mesas and wells and found out that the width of the mesa and the depth of the trenches are critical for good lateral ordering of monolayers of spherical microdomains. The depth of the trench has to be equal or greater than the height of one layer of spheres in order to obtain good lateral ordering. [49]

The interfacial interactions between the polymer and the pattern wall and bottom become important when aligning block copolymers exhibiting lamellar or cylindrical morphologies. *Sundrani et al*. aligned PS cylinders of PS-*b*-PEP block copolymers oriented parallel to the substrate within a grating pattern. They noted that alignment was achieved by preferential interaction of the PS block with the substrate and the sidewalls of the throughs, which induced parallel orientation of the microdomains as well as templated the lateral alignment of PS cylinders along the edges of the pattern. [52], [55]

Similarly, cylinders oriented perpendicular to the substrate can be also be aligned by using patterned surfaces. The only modification needed is the treatment of patterned substrates with a surface-neutralizing random copolymer layer prior to the addition of the block copolymer. It has been noticed that when the wall spacing does not match the lattice spacing of the microdomains ($W \neq nL_0$), the lattice spacing of cylindrical microdomains expands or compresses to fit within the confined channel. [56]

It has also been demonstrated that the perpendicular alignment of cylinders can be achieved in topographical relief structures without applying the neutralizing layer. If the dimensions of the structures are small enough (length $\approx 2L_0$), the strong confinement from the templates overcomes the affinity difference between the different blocks to the substrate. *Bao et al.* fabricated square wells into a silicon wafer with 126 nm sides and pattern depth of 50 nm and demonstrated the patterning of 2 x 2 lattice of 4 contact holes (diameter 25 nm) by using the self-assembly of cylindrical PS-*b*-PMMA block copolymer. PMMA cylinders arranged perpendicular to the substrate without the surface neutralizing brush layer due to the strong confinement. This explanation was in line with the notion that 5 x 5 square lattices cannot be obtained in a square well due to the decreased surface energetic effect that the larger wells have. [45]

The alignment of lamellae-forming block copolymers have been the object for several studies and it has been well established that interactions between the blocks and the walls govern the orientation of microdomains, and the commensurability between the wall separation and the polymer period affects domain spacing. Nealey and his group stated that to align the perpendicular lamellae within the patterned trenches, the bottom surface should have a neutral interaction with both blocks while the sidewalls should have preferential wetting by one block. If the wetting of both the bottom and the sidewalls is preferential to one block, lamellae are oriented parallel to the bottom, while neutral wetting of walls and bottom results in lamellae perpendicular to both the bottom and sidewalls. [54] This behavior is shown in Figure 2.11.

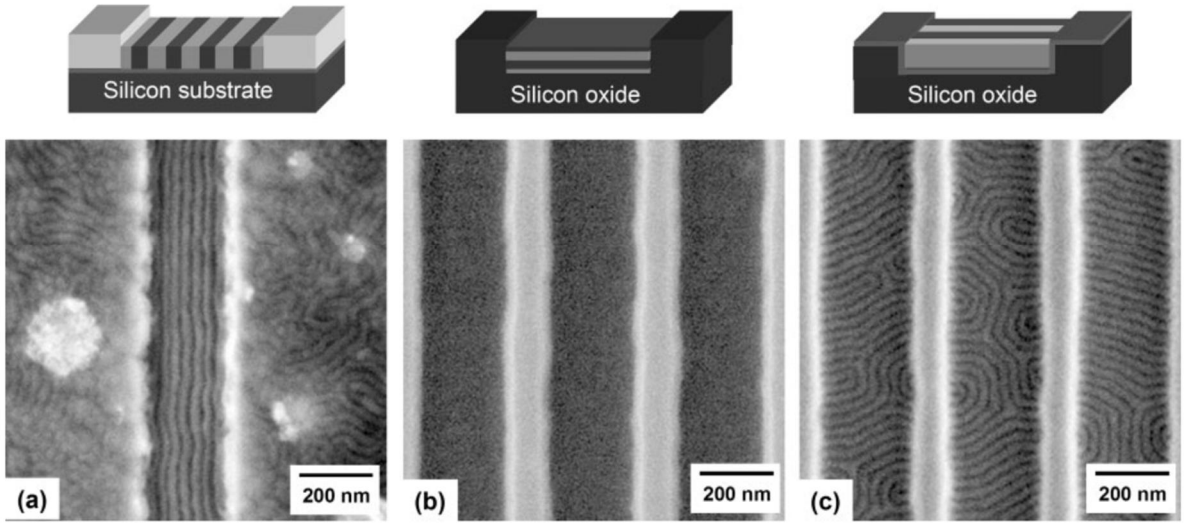

Figure 2.11. *Lamellar structures of symmetric PS-b-PMMA block copolymers on topographically patterned substrates. a) The sidewalls of gold patterns are preferentially wet by PS and the bottom groove exhibits neutral wetting behavior to both blocks. b) SiO2 substrate is preferentially wet by PMMA block and the alignment oriented parallel to the bottom of the groove. c) topographic pattern in b) is treated with a neutral brush to obtain lamellar domains oriented perpendicular to both the substrate and the pattern sidewalls. [54]*

The drawbacks in utilizing topographical prepatterning for directing the self-assembly of block copolymers is the loss of valuable substrate area due to the patterning and the costly instruments needed for the lithographic prepatterning. [57]

2.4.2 Chemical prepatterning

Chemical prepatterning technique exploits the surface-polymer interactions to quide block copolymers to phase separate in a controlled manner. As noted before, chemically different blocks in a block copolymer have different affinities to the substrate that it is in contact with and one of the blocks will preferentially wet the surface. Chemical prepatterning method is based on the patterning of an imaging layer to modify its surface chemistry in some areas. An example of a chemical prepatterning process is shown in Figure 2.12. A low molecular weight polystyrene (PS) brush is added onto a substrate by spin coating and thermal annealing. This thin layer of polystyrene acts as the imaging layer. After that, a resist is spin coated on top of the PS brush and patterned with a conventional lithography method, for example electron beam (e-beam) [58], extreme ultraviolet interference (EUV) [59] or Argon fluoride laser (ArF) projection lithography [60]. Once developed, an oxygen plasma etch is used to generate the nanopattern through the photoresist and into the PS imaging layer. This step modifies the exposed areas of the PS layer to be oxygen rich and therefore prefer the polar PMMA block in the PS-*b*-PMMA block copolymer. The rest of the resist is removed and the PS-*b*-PMMA block copolymer is then spin coated on top of the chemical nanopattern and

annealed above the glass transition temperature of the block copolymer to allow the microphase separation and self-assembly according to the underlying chemical pattern.

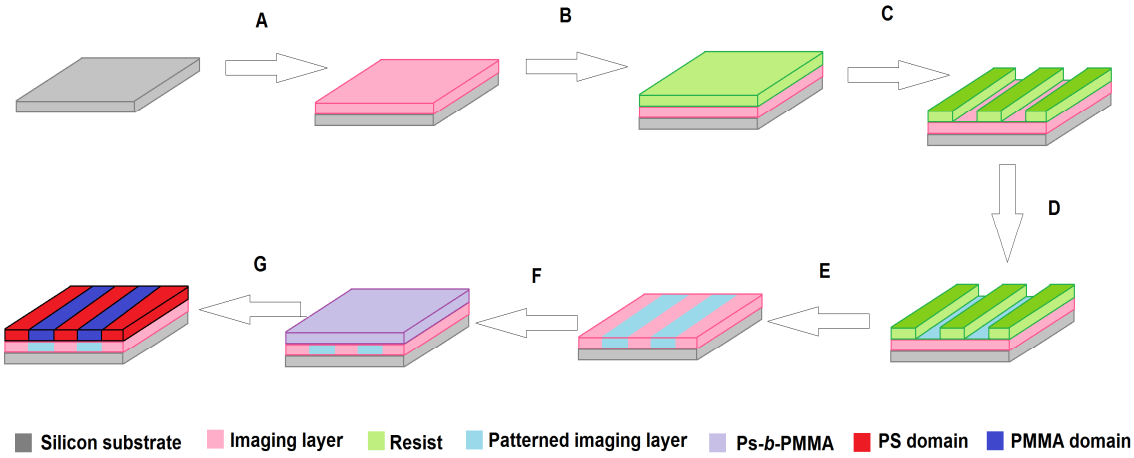

Figure 2.12. *Chemical prepatterning process for PS-b-PMMA block copolymer. An imaging layer is applied to the silicon surface (A) and the resist layer is spin coated on top of the imaging layer (B) and patterned with some lithography method (C). The underlying imaging layer is oxidized from the areas not covered by resist by O_2 plasma etch step (D) after which the resist is removed (E) and the block copolymer is applied on top of chemically the patterned imaging layer (F). The microdomain formation follows the guiding pattern in the imaging layer (G).*

Chemical prepatterning has been used with lamellae-forming block copolymers to produce a variety of features such as dense lines, bends, line terminations and T-junctions [61] A similar method can also be used with cylinder forming block copolymers to produce linear arrays of cylinders [60], to align the cylinders in a square array [44] or to enhance the pattern periodicity in the hexagonal array. Resolution enhancement by density multiplication means that the density of block copolymer features exceeds the density of the prepattern features by an integer multiple. Defect free assemblies of hexagonally packed cylinder with up to 4:1 density multiplication have been achieved. [58] [62] Scanning electron microscope (SEM) images of pattern rectification and density multiplication processes before and after the addition of a polymer layer are shown in Figure 2.13.

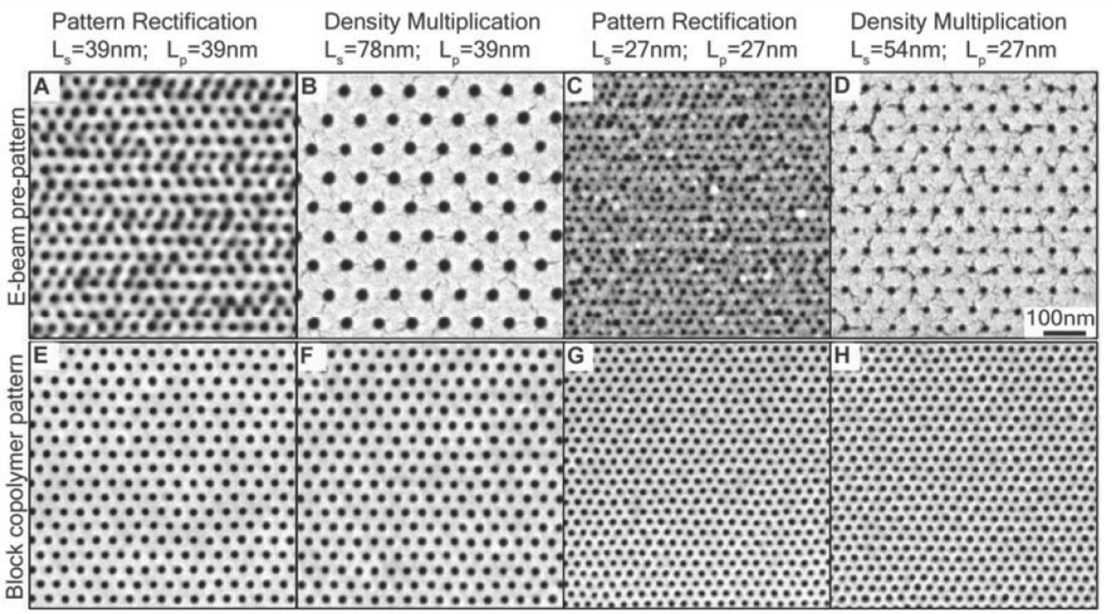

Figure 2.13. *Pattern rectification and density multiplication by chemical prepatterning with e-beam lithography. Images A-D represent SEM images of developed e-beam resist with varying lattice pitches L_s. Corresponding SEM images (E-H) of the annealed block copolymer film on top of the chemical prepattern. The lattice pitch of the block copolymer L_p is 39, 39, 27 and 27 nm respectively. Images E and G illustrate pattern rectification and F and H density multiplication processes. [62]*

The substrate surface chemistry and the dimensions of the guiding pattern dictate the quality of the assembly generated through density multiplication. It has been shown that the best assemblies of both lamellar and cylindrical block copolymer domains are achieved when the substrate surface is weakly preferential to one of the copolymer blocks. [62], [63]

3 LITHOGRAPHY

The literal meaning of the word lithography is “writing on stones” and it derives from the Greek words *lithos* (stones) and *graphia* (to write). Today, the stones are silicon wafers or other substrates onto which the patterns are written with a light-sensitive polymer called photoresist. The aim is to form three-dimensional relief images on the photoresist for a subsequent transfer of the pattern into the substrate.

The lithographic methods are widely utilized in the semiconductor industry for fabrication of microscale (microlithography) or nanoscale (nanolithography) structures. The development of microlithography was initiated by the development of integrated circuits (ICs) that created a need for high volume and low cost method of small pattern replication on a substrate. Lithographic methods can be divided into several categories. Sometimes the patterns are written directly on the substrate in question. More often, however, the patterns are written on a plate. This plate acts as a photomask through which the light beams shine through to transfer the pattern into the photoresist layer on the substrate. This process is called optical lithography. [64]–[66]

Although these traditional lithographic methods are useful and they are widely applied, still significant challenges exist in patterning unusual systems and materials (e.g. in biotechnology and plastic electronics), structures with nanometer dimensions, large areas in single step or nonplanar surfaces. Soft lithography has been studied for its potential to overcome some of the limitations of photolithography. Soft lithographic methods all share the common feature that they use a patterned elastomer as the mask, stamp or mold. The term “soft” is used because these techniques utilize flexible organic molecules and materials rather than the rigid inorganic materials commonly used in the traditional lithographic methods. [9], [10]

In this chapter, the lithography techniques utilized in this Thesis are briefly introduced.

3.1 Electron beam lithography

The prepatterning method for block copolymer directed self-assembly used in this thesis has been electron beam lithography (EBL), which is a direct write method that is often used to pattern photomasks for optical lithography and masters for nanoimprint lithography. EBL technique consists of a beam of electrons scanning across a surface covered with a resist film. The resist is cured due to interaction with the electron beam. EBL is a precise method of patterning over small areas of the wafer, capable of very high resolution almost to atomic level, exhibits low defect density due to lack of contact with the mask and is a also very flexible since it can work with a variety of materials and almost

infinite number of patterns. The main drawbacks of the EBL are low throughput and high capital cost. The price of the machinery can be lowered by adding an electron beam lithography system to an already existing scanning electron microscope (SEM). Because of the slow speed of processing, EBL is mostly used for research and development purposes. [66], [67]

The electron beam lithography system is composed of four basic elements: an electron column, a XY-laser controlled mechanical stage, a central processing unit to control the stage, a blanker for the electron beam and the substrate holders. [67]. A block diagram of a typical EBL tool is shown in figure 3.1.

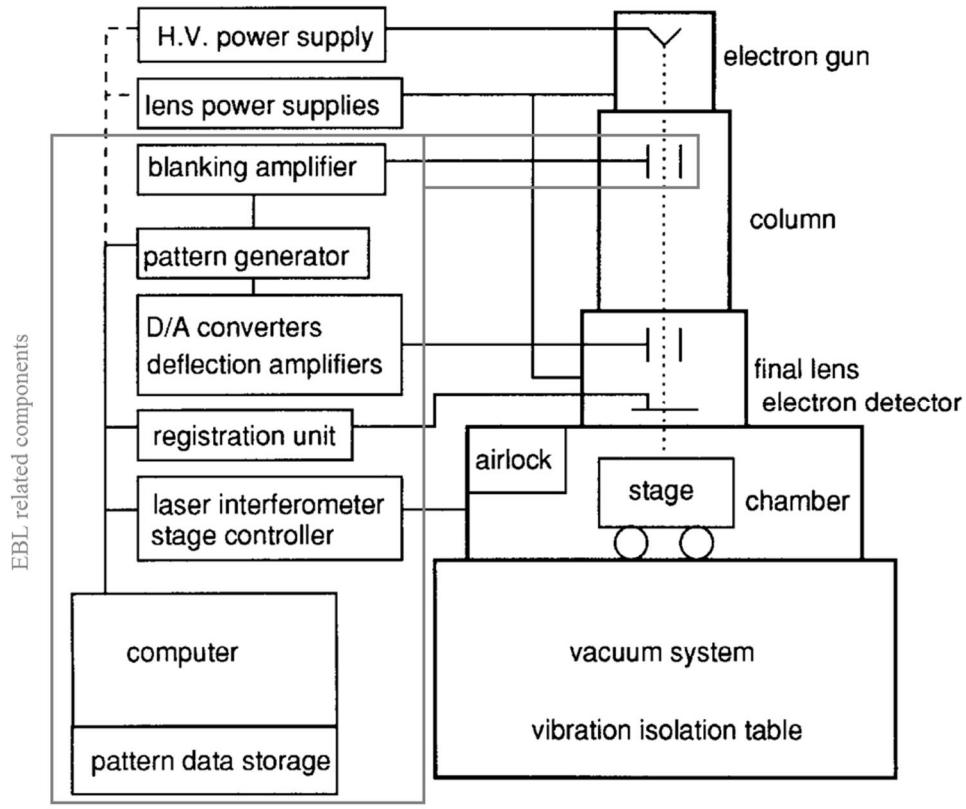

Kuva 3.1. *A block diagram of the major components in a typical electron beam lithography system. The blocks surrounded by the light grey rectangle are related only to the EBL system and the rest of the system is parts of scanning electron microscope (SEM) equipment. [66]*

The forming of the electron beam takes place in the electron gun placed at the top of the column. Underneath, there is a stage for moving the sample around and facilities for loading and unloading it. A vacuum system connected to the chamber is needed to maintain an appropriate vacuum level throughout the system. The beam is controlled by magnets along the column using a computer. The electrons in the electron source can be emitted either by thermal emission, which means heating a conducting material to the point where the electrons have sufficient energy to overcome the work function barrier of the conductor or by field emission in which a sufficiently high electric field allows the electrons to tunnel through the barrier. [66]

The EBL process is based on exposing a resist to a sharp, narrow beam of electrons, which are accelerated using a high voltage. There are two kinds of resists. In positive resists, the exposure to the electron beam reduces the molecular weight of the resist by cutting the chemical bonds in the resist molecules so that these exposed regions become soluble to a developer solvent. On the contrary, when using a negative resist, the beam exposure induces the cross-linking of the molecules which means increasing the molecular weight in the exposed areas. Then developer solvent removes the unexposed areas with lower-molecular weight. After the development step the created pattern can be transferred to the underlying substrate by etching methods such as reactive ion etching (RIE). A typical positive resist for EBL is poly(methyl metacrylate) (PMMA) and an example of a negative resist is poly(vinylmethyl siloxane) (PVMS). [67] Figure 3.2 is a schematic representation of the electron beam lithography process, which also shows the difference between the positive and the negative photoresists.

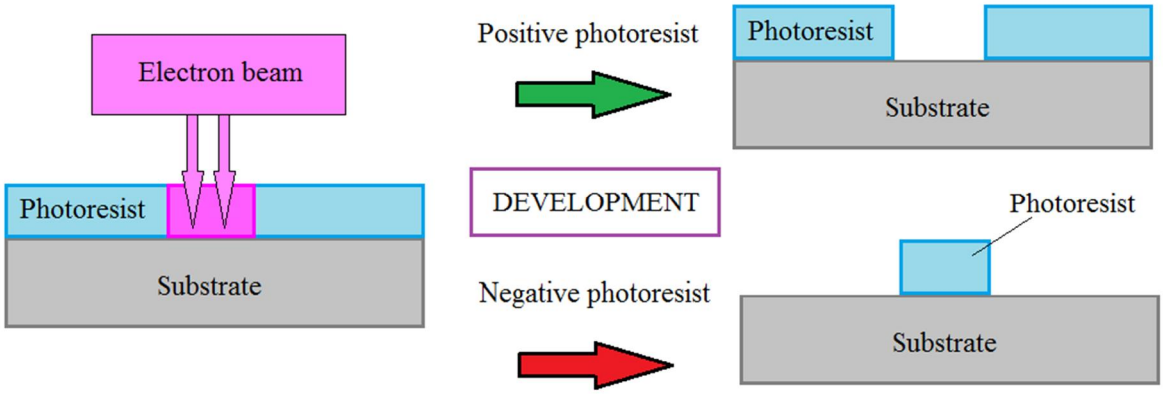

Figure 3.2. *Electron beam lithography process with positive or negative photoresist.*

It has been shown that the resolution limit of EBL can be pushed below 10 nm and 3-5 nm wide lines have been successfully patterned onto PMMA resist layer at a pitch of 30 nm. [68]

3.2 Soft lithography and nanoimprint lithography

Although photolithography has been the most successful technology in microfabrication, problems exist for example in the resolution limit set by optical diffraction and the restricted variety of materials that can be used as resists and substrates. To serve the demand for smaller and smaller, easily produced patterns, a number of non-photolithographic techniques have been developed, one of which is soft lithography. The basic principle in soft lithography is to fabricate an elastomeric stamp or mold that transfers the patterns to the substrate. Microcontact printing (μCP) [69], replica molding (REM) [70], microtransfer molding (μTM) [71] and nanotransfer printing (nTP) [72] are some examples of the soft lithographic methods available.

In microcontact printing the elastomeric stamp is used to generate micropatterns of self-assebled monolayers (SAMs) by contact printing. Self-assembly means spontaneous organization of molecules into stable and well oriented structures. The final structure is close or at thermodynamic equilibrium and as of that it rejects defects. Self-assembly can also be found in many structures in nature. For example the folding of proteins and the formation of DNA double helix are biological self-assembly processes. [9]

The basic procedure of microcontact printing is represented in Figure 3.3. The elastomeric stamp is used to transfer a self-assembled layer of molecules of the "ink" to the surface of the substrate by contact. The contact times required are usually only a few seconds and there is no need for high pressure, only an even contact between the stamp and the substrate is required. After printing, the patterned SAMs can be used as ultrathin resists in selective etching or as templates to control the wetting, dewetting, nucleation, growth or deposition of other materials.

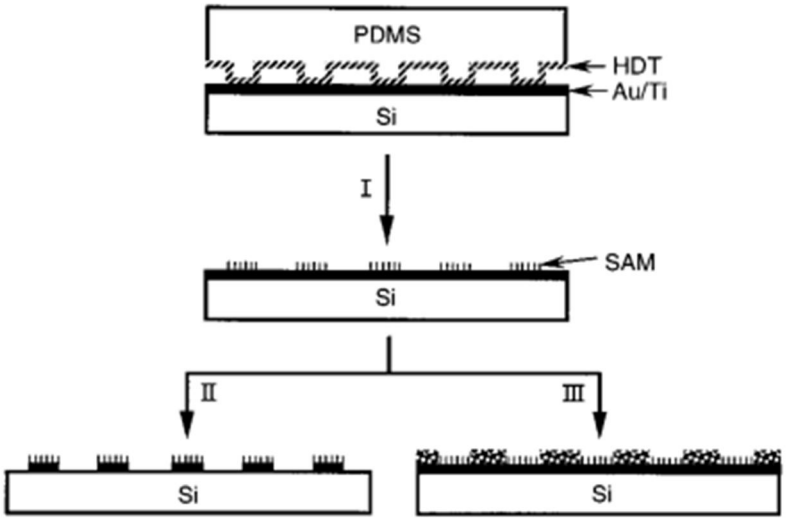

Figure 3.3. *Microcontact printing process. The PDMS stamp is inked with hexadecanethiol (HDT) and the ink molecules are transferred to the gold or titanium covered silicon substrate to form a SAM on the contact spots. After the contact, the unpatterned areas can be etched off (II) or a different SAM can be formed on unpatterned areas to fill in the holes (III).[9]*

Microcontact printing was first demonstrated for SAMs of alkanethiolates on gold [69] but other inks and substrates can also be used. For example *Grothe et al.* used microcontact printing to fabricate microscale structures of silver on glass substrate. They selectively printed 3-mercaptopropyltriethoxysilane (MPTES) molecules on the activated glass substrates followed by subsequent electroless metallization of silver on top of the MPTES layer.

Nanoimprint lithography (NIL) has very much in common with the soft lithographic methods as it utilizes soft elastomeric stamp to create patterns on substrates. The difference here is that a resist much like the ones used in photolithography is spread to the surface of the substrate. The stamp is then pressed in contact with the resist so

that the resist adjusts to the pattern on the stamp. After this the resist is cured either with UV-light (UV-NIL) or by heating and cooling (thermal NIL) to transfer the stamp pattern into the resist. After the stamp and the substrate have been separated, the relief pattern can be etched into the substrate with the resist as an etch mask. [11], [73]

High resolution stamps for μCP and NIL can be produced by replica molding from masters that have been previously patterned by conventional lithography. The liquid prepolymer of an elastomer is cast on to the relief-patterned master and hardened by heating and finally carefully separated from the master. One master can be used to fabricate multiple stamps and each of the stamps can last for several printing cycles. Therefore, the conventional lithographic methods for master fabrication are not required often. Poly(dimethylsiloxane) (PDMS) is the elastomer used for stamps in most demonstrations since most of its properties are instrumental for high quality pattern formation. PDMS conforms well to the surface of the substrate due to its elasticity and spreads well even over complex structures. It is also chemically inert and durable, which enables the stamps to be used multiple times. However, the elastic character can also cause problems. If the aspect ratio of the relief pattern is too large (the pattern depth is much larger than the width), the PDMS microstructures may fall under their own weight or collapse during the printing process. Similarly, if the aspect ratios are too low (the pattern width much larger than depth), an effect called sagging may take place when the structures are not able to withstand the compressive forces during printing. [9], [10] These two failure scenarios are represented schematically in Figure 3.3.

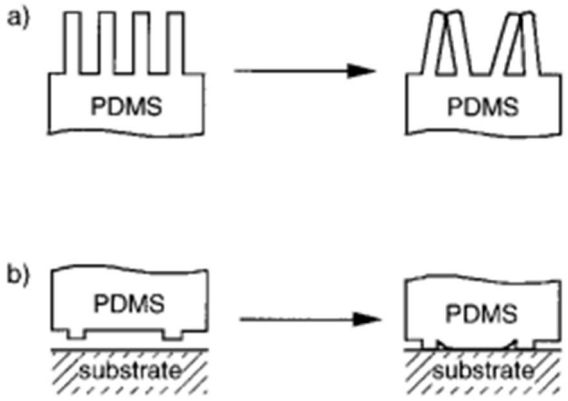

Figure 3.4.*Typical problems with PDMS stamps: a) collapsing happens when the aspect ratio of the relief features is too large and b) sagging happens during the printing process on PDMS stamps with too low aspect ratio. [9]*

Delamarche et al. investigated the appropriate aspect ratios and showed that defect free PDMS stamps can be obtained when the aspect ratios are between 0.2 and 2. [74]

4 COLLOIDAL QUANTUM DOTS

The aim for the processes developed during this thesis is to achieve selective deposition of colloidal quantum dots by first fabricating a stamp using a master created by block copolymer lithography. This stamp is subsequently used in a microcontact printing process to transfer (3-Mercaptopropyl)trimethoxysilane (MPTMS) molecules on top of a silicon substrate. These MPTMS printed areas would then bind quantum dots by chemical forces described later and thus selective deposition of the quantum dots on the areas covered with MPTMS would be achieved. The structure and the properties of the colloidal quantum dots are described in more detail in this chapter.

Quantum dots (QDs) are nanoscale crystals of semiconducting materials, sometimes termed “artificial atoms” due to the relatively small number of electrons and many body effects by which the properties of the dot could be dramatically changed by adding just one electron. A quantum dot consists of a small, semiconductor core (1 - 10 nm in diameter). A typical quantum dot is composed of a mixture of group II and VI materials, such as cadmium and selenium (CdSe) as a core, a wider-bandgap semiconductor shell (e.g. cadmium sulphide CdS or zinc selenide ZnSe) surrounding the core and a coating of organic ligands. Some quantum dots consist of only the core and ligands and lack the shell structure altogether. A schematic picture of the general structure of a quantum dot is represented in Figure 4.1.

Kuva 4.1. *The structure of a quantum dot. [75]*

Quantum dots can be categorized by their synthetic route to epitaxial and colloidal quantum dots. Epitaxial QDs are synthesized by methods of epitaxial growth, whereas colloidal QDs are synthesized by chemical approaches, usually in a solution. Epitaxial quantum dots are bound on the substrate they are grown onto unlike colloidal quantum dots, which are freestanding in a selected solvent. This enables a large number of chemical post-processing and thin-film assembly steps, which makes the colloidal quantum

dots interesting for many applications. Moreover, the size of colloidal quantum dots is easy to control during the synthesis and the desired quantum-confinement effects are stronger than in epitaxially grown QDs. [76]

The unique properties of QDs are due to their small size. When photon is absorbed by thedot, an electron form the valence band is promoted to the conduction band, thus generating an electron-hole pair. This electron-hole pair is called an exciton. Unlike in the bulk, where excitons can have a range of energies within a continuous band, in the nanoscale the excitons are confined on the order of the bulk semiconductor's Bohr exciton radius (e.g. 5.6 nm for CdSe) and this leads to quantization of the bulk energy levels, resulting in atomic emission-like spectra. This means that as each excited electron recombines with a hole, it emits a photon with a specific, predictable wavelength. Another result of this confinement is that the QD's bandgap increases as its size decreases, leading to a decrease in emission wavelengths. This tunable bandgap is the most important quality of the QDs. The spectral tunability can be extended through the chemical composition and stoichiometry of the QD. [76]

The ligands (sometimes also referred to as surfactants or capping molecules) are required during the colloidal synthesis of quantum dots to control the size and shape of the QD by accelerating or inhibiting growth of some facets. [75] [77] In addition, the solubility of a QD depends on the hydrophobicity/hydrophilicity of the ligands. Typically hydrophobic ligands are used during the synthesis. The chemistry of ligands also plays an important role in the formation of Langmuir monolayers [78] and the assembly of the quantum dots on surfaces. Attachment of quantum dots on surfaces is important for example in solar cell applications. In specific cells, TiO_2 surfaces can be modified by 3-mercaptopropyl trimethoxysilane (MPTMS) or 3-aminopropyl-methyl diethoxysilane (APMDS) to contain a thiol or amino terminated surfaces, respectively. This facilitates the binding with the CdSe QD ligands that contain carboxylic acid groups to the surface by bonding with the thiol or amino groups attached to the TiO_2 surface. [79] Another group used bifunctional linker molecules that contained carboxylate and thiol functional groups to facilitate the binding of CdSe QDs to TiO_2 (Figure 4.2). The thiol end of these bifunctional linkers attaches to the oxide leaving the carboxylic end free to react with the ligands surrounding the QD by ligand exchange reaction. [80]

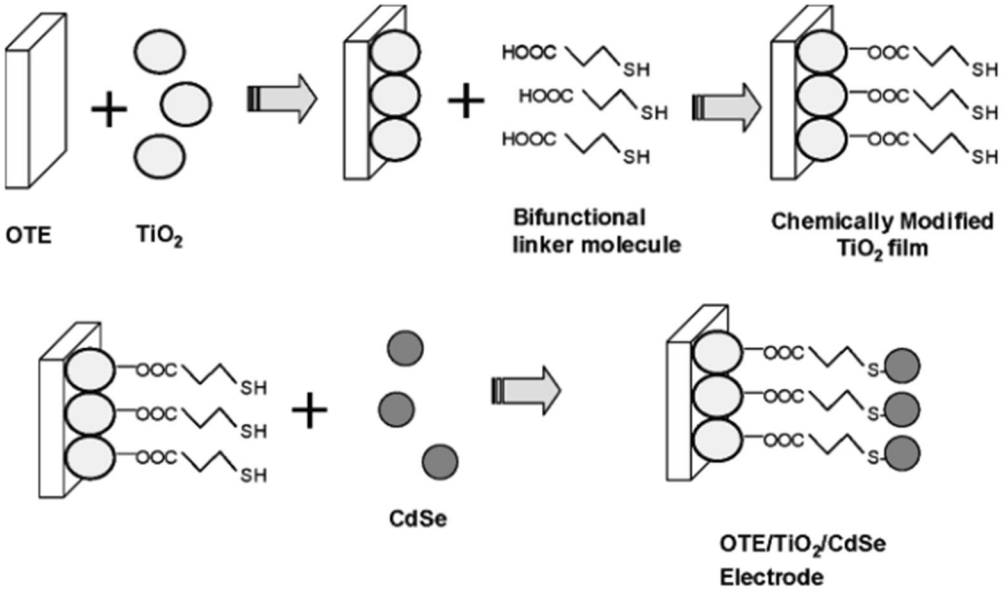

Figure 4.2.*Linking CdSe quantum dots to TiO_2 surface via bifunctional (COOH-R-SH) linker molecules. [80]*

Quantum dots have applications in optoelectronics and biomedical technologies such as light emitting devices (LEDs) [81], solar cells [82], photodiodes [83] and in vivo and in vitro imaging, sensing and labeling techniques [84].

5 RESEARCH METHODS AND MATERIALS

The measurements in this thesis were carried out at the Tampere University of Technology during autumn 2013 and spring 2014. The major part of the measurements took place in the Optoelectronics Research Centre (ORC) but the fluorescence microscope measurements were performed at the Department of Chemistry and Bioengineering.

5.1 Block copolymers

The block copolymer used in this thesis is polystyrene-*block*-polymethyl metacrylate (PS-*b*-PMMA). Although a variety of diblock copolymers can be used, PS-*b*-PMMA was chosen since it is a great choice for lithographic applications because the cylindrical PMMA domains can be selectively removed using oxygen plasma or acetic acid. The resulting porous PS films can serve as templates for nanostructure formation [85]. The structural formula of PS-*b*-PMMA is shown in Figure 5.1.

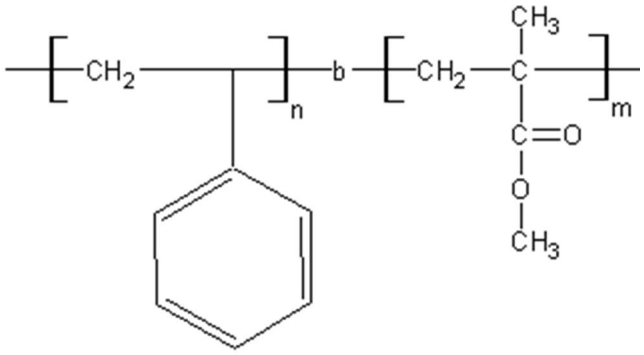

Figure 5.1. *The structural formula of PS-b-PMMA. The first block is polystyrene and the second one is polymethyl metacrylate.*

All of the block copolymers were purchased from Polymer Source Inc. Two PS-*b*-PMMA BCPs of different molecular weights were used. The styrene fraction of each BCP was about 70 %, which is the composition required for a cylindrical morphology. Details of the polymers used are listed in Table 5.1. A solution of 1 wt% of PS-*b*-PMMA in toluene was prepared by weighing 0.044g of polymer and diluting it in 5 ml of toluene. Toluene was purchased from Sigma Aldrich and used as received.

***Table 5.1**. Molecular weights (M_n) of the block copolymers and their PS and PMMA domains, polydispersities (PDI), and the PS volume fractions of the block copolymers used.*

Name	$M_n \times 10^3$ (g/mol)	PS $M_n \times 10^3$ (g/mol)	PMMA $M_n \times 10^3$ (g/mol)	PDI (=M_w/M_n)	PS volume fraction
P(67.1)-SMMA	67.1	46.1	21	1.09	0.69
P(101.5)-SMMA	101.5	68	33.5	1.08	0.67

Two different kinds of imaging layers were used. A neutral layer was produced using a random copolymer of polystyrene and polymethyl metacrylate (PS-*r*-PMMA) with a hydroxyl terminated end. Hydroxyl terminated end is needed to graft the random copolymer to the oxygen layer of the substrate. The molecular weight of the random copolymer PS-*r*-PMMA was 9.7×10^3 g/mol and the polydispersity index (PDI) 1,45 The composition of the random polymer was similar to that of the block copolymers and it contained 60 % polystyrene. The structural formula of PS-*r*-PMMA used in this Thesis is shown in Figure 5.2.

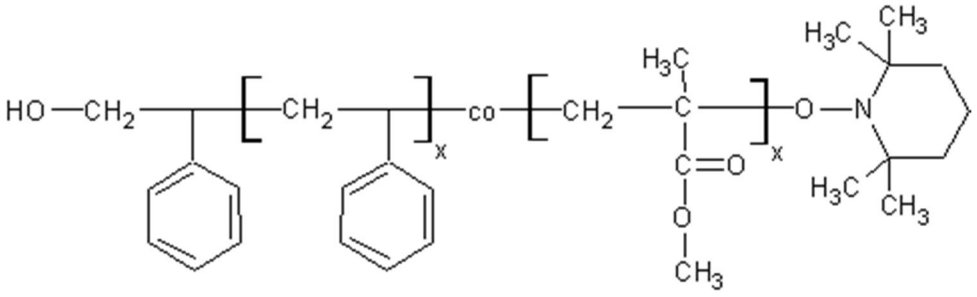

***Figure 5.2.** PS-r-PMMA, α-Hydroxyl-ω-Tempo moiety terminated.*

PS-*r*-PMMA was used as 2 wt% solution in toluene prepared by weighing 0.089 g of polymer and diluting it in 5 ml of toluene (Sigma Aldrich).

5.2 Block copolymer sample preparation

The following process was used for the formation of self-assembled block copolymer thin film of cylindrical PS-*b*-PMMA (PS fraction ~70%) where the cylinders lie perpendicular to the substrate. The substrates used in all block copolymer processes were thin silicon substrates. For some of the substrates, a 10 to 30 nm thick silicon oxide layer (SiO_2) was deposited on top of the substrate by plasma-enhanced chemical vapor deposition (PECVD).

The silicon wafers (with or without the deposited SiO_2 layer) were cleaned by immersion in hot piranha solution (4:1 H_2SO_4 and H_2O_2) for 10 minutes followed by oxygen plasma activation. Besides cleaning the substrate, the purpose of this procedure was to form of a thin native oxide layer as well as OH groups at the surface of the sub-

strate. [86] To obtain surface perpendicular domain orientation in block copolymer layer, a neutralizing imaging layer has to be applied first. [33] For this purpose, a 2.0 wt% solution of random copolymer (PS-*r*-PMMA) in toluene was spin coated (1500 rpm, 30 s) onto the cleaned substrates. The polymer-coated substrates were then annealed in vacuum at 175 °C, well above the glass transition temperature (T_g) of both PS and PMMA, to allow the terminal OH groups in the random copolymer to diffuse to and react with the native oxide layer on the substrates. After 72 hours, the substrates were removed from the oven and spin washed with toluene several times to remove unattached polymer chains. The thickness of the crafted random polymer layers measured by ellipsometry was ~5 nm.

Next, the selected block copolymer was spin coated on top of the surface neutralizing random copolymer layer grafted onto the substrate. The concentration of the BCP solution was 1 wt% and the spin speed 3000-3500 rpm. After the spin coating the samples were annealed at 185 °C in vacuum for 48 hours. Finally, the PMMA domains were etched off by reactive ion etching (RIE) with oxygen and argon gases. The detailed process flow for the block copolymer self-assembly process on unpatterned surfaces is presented in Appendix 3.

5.3 Electron beam lithography

The electron beam lithography equipment at ORC is Raith Elphy Plus apparatus that is attached to Carl Zeiss SMT SEM Ultra-55 scanning electron microscope unit (Figure 5.3). The aperture size used for patterning was 20 or 10 µm for the smallest patterns in chemical patterning and the accelerating electron voltage 10 kV in all the patterning processes. The resist used in all the patterning processes is positive 950K PMMA e-beam resist AR-P 672.03 purchased from ALLRESIST GmbH. [87]

Figure 5.3. *SEM and EBL instruments in Optoelectronics Research Center.*

In Figure 5.3 the EBL apparatus is located in the left and SEM instrument in the middle, next to the computer monitors.

5.3.1 Topographical prepatterning

Topographical prepatterning was performed on a clean substrate before applying any of the polymer layers to get the topographical relief on the substrate first. A 200 nm PMMA e-beam resist layer was spin coated on the cleaned silicon substrates and baked on a hot plate for 2 minutes. The e-beam patterning of the desired geometries was performed next.. After the patterning, the resist was developed by immersion in a 3:1 mixture of methyl isobutyl ketone (MIBK) and isopropyl alcohol (IPA) for 30 s followed by 30 s rinse with IPA. The patterns were transferred to the underlying silicon substrate by reactive ion etching using SF_6 and O_2 plasmas. The remaining PMMA resist was removed by sonication in 40 °C toluene for 20 minutes. For some of the samples a thin (~10 nm) silicon dioxide layer was grown on top of the relief pattern with PECVD. After this the general block copolymer process described in the beginning of Chapter 5.2 was applied. The detailed process flow for the topographical patterning process is presented in Appendix 2.

The patterning of the square well structures differs a little from the trench patterns. As noted by *Wong et al.* the surface neutralizing bottom layer is not required to obtain surface perpendicular cylinders inside the square wells because the confinement effect from the pattern walls forces the cylinders upright since there is no space for them to lie parallel to the surface [45]. Because no random copolymer layer is needed to be grafted onto the silanol groups, there is also no need for the SiO_2 layer. Thus, the e-beam patterns were directly written onto the cleaned silicon substrates and after patterning, etching and resist removal, the PS-b-PMMA block copolymer was directly spin coated onto the patterned silicon substrates.

To achieve neutral wetting behavior in the bottom of the features but PS preferential wetting in the sides, the topographical structures were alternatively prepared from gold on top of the neutral imaging layer [54]. Gold sidewalls were fabricated by a lift-off technique. First the PMMA resist was spin coated on top of the already annealed PS-r-PMMA imaging layer followed by e-beam patterning of trenches of varying lattice spacing. The underlying idea in a lift-off process is to create vertical or even negative side-wall profiles in the resist that can be easily removed by solvent. Here the slightly negative sidewalls were achieved by extending the development time of PMMA resist after the e-beam patterning from 30 to 50 seconds. After the resist development, 5 nm of chromium and 40 - 50 nm of gold were evaporated on top of the resist layer. This was followed by the lift-off step by ultrasonicating the samples in 40 °C toluene for 20 minutes which removed the resist but left the gold patterns in place. The detailed process flow for the topographical patterning process with gold is presented in Appendix 3.

5.4 Microcontact printing

Microcontact printing was carried out in EVG 620 mask aligner using a stamp made from hard poly(dimethylsiloxane) elastomer (h-PDMS) . The EVG 620 is an optical lithography system with a nanoimprint lithography (NIL)/microcontact printing (µCP) tool option installed (Figure 5.4).

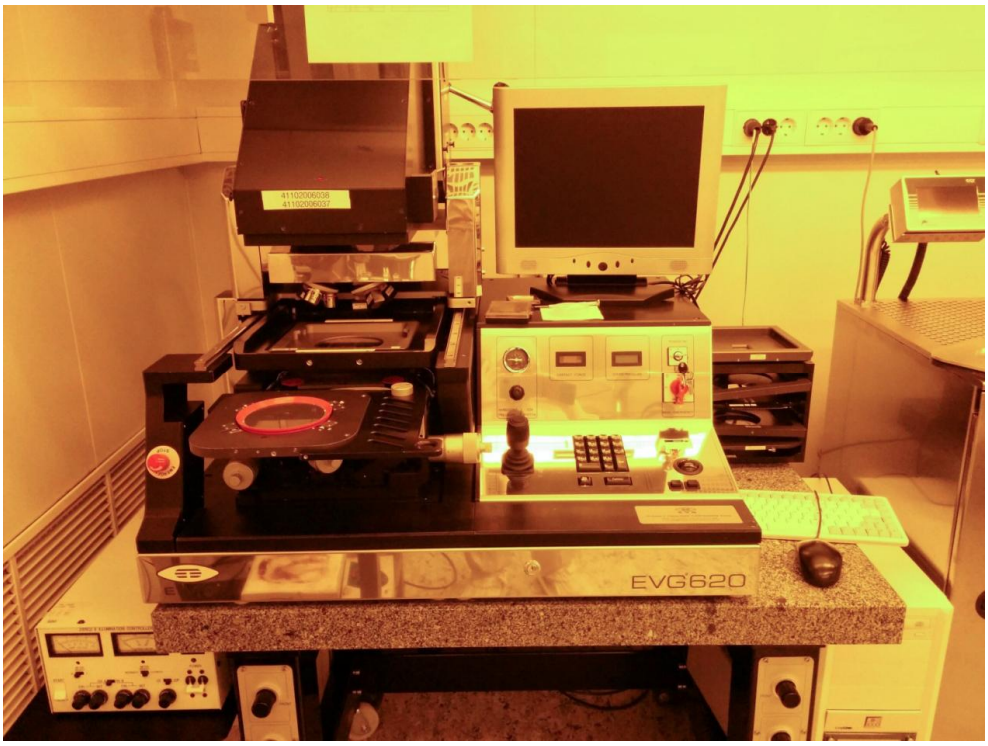

Figure 5.4. *EVG 620 Mask aligner that was used for microcontact printing and nanoimprint lithography in this Thesis.*

The system used for microcontact printing consists of a chuck that uses vacuum to attach the sample to the holder and a vacuum ring that creates and maintains the vacuum

during the printing process. In the first step, the stamp and the sample are loaded into the holders. There are small pins in the sample holder that hold the sample and the stamp a very close to each other without touching so that they can be aligned using the magnifying camera in the system. After the alignment step, the stamp and the substrate are brought into contact. For microcontact printing, there is no need for high pressure and only a contact between the sample and the stamp is adequate to achieve the flow of the molecules from the stamp to the substrate. The tricky part is to determine the suitable force to achieve the contact without too much pressure. The printing process in this thesis was done at the pressure of 300 µPa and the printing time was 500 s.

A nanoimprint lithography (NIL) process was used for evaluation of the quality of the stamps fabricated from block copolymer masters. NIL process was also performed using the EVG 620 mask aligner. Both µCP and NIL employ similar stamps made of h-PDMS. The difference between these two is that in µCP the patterns forming are monolayers of molecules attached to the surface of the substrate via chemical forces whereas in NIL the stamp pattern is molded into UV-resist spin coated on top of the substrate. The resist is hardened by UV exposure to create a replica of the relief pattern on the stamp to the substrate. The main differences in the NIL process compared to µCP are that in NIL the substrate is covered with the resist and after the contact between the stamp and the substrate, the UV-exposure step is added. The resist used for NIL in this thesis was mr-UVCur from Micro Resist Technology GmbH. [88]

5.4.1 Stamp preparation

The soft stamp materials commonly used in ORC are Ormostamp (micro resist technology GmbH) and hard or soft poly(dimethylsiloxane) elastomers (h-PDMS, s-PDMS). s-PDMS is not good for copying patterns with small dimensions [89] and therefore it is generally used as a soft mattress to make the stamp structure more flexible. The general configuration of the stamp consists of a thick glass sheet topped with an s-PDMS mattress and finally a smaller, thin glass sheet with the patterned stamp material (Figure 5.5).

Figure 5.5. *The configuration of the stamp used in this thesis. The stamp consists of a thick glass sheet topped with a soft PDMS mattress to give the stamp more flexibility. The two topmost layers are a thin glass sheet onto which the patterned elastomeric stamp material is attached.*

The choice for the elastomeric stamp material in the experiments here was h-PDMS as it adjusts well to smaller patterns. Before applying the elastomeric stamp material, the masters are coated with an antiadhesion layer to make the separation of the ready stamp from the master easier [90]. The antiadhesion chemical used in this thesis was perfluorodecyltrichlorosilane (FDTS) (Figure 5.6) and it was applied by evaporation in a vacuum chamber.

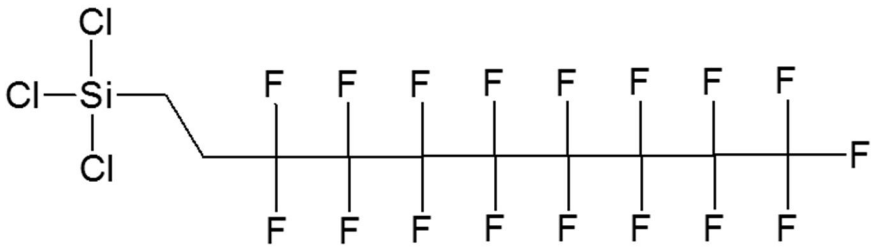

Figure 5.6. *Perfluorodecyltrichlorosilane (FDTS) molecule used for obtaining an antiadhesion layer on top of the master before the stamp fabrication.*

After the formation of the antiadhesion layer, the h-PDMS material was prepared by mixing two different prepolymers VDT-731 and HMS-501 both purchased from ABCR GmbH. The polymerization process was accelerated by adding a drop of platinum catalyst AB146697 (ABCR GmbH) and the hardening of the material was slowed down by inhibitor LA16645. The thickness of the h-PDMS layer can be modified by varying the spin speed or further by diluting the polymer mixture with toluene. [11], [91] Table 5.2 includes a detailed list of all the substances uses for h-PDMS stamp preparation.

Table 5.2. *The chemicals used for the fabrication of h-PDMS soft stamps for microcontact printing and nanoimprint lithography [11].*

Brand name	Chemical name	Amount	Role in the mixture
VDT-731	trimethylsiloxy terminated vinylmethylsiloxane-dimethylsiloxane copolymer	3.4 g	Prepolymer
HMS-501	trimethylsiloxy terminated methylhydrosiloxane-dimethylsiloxane copolymer	0.75 g	Prepolymer
AB146697	Platinumdivinyltetramethyldisiloxane complex in xylene	1 drop	Catalyst
LA16645	2,4,6,8 - Tetramethyl - 2,4,6, 8 – tetravinylcyclotetrasiloxane	4 drops	Inhibitor
Toluene		5 g	Thinner

After the chemicals were mixed, the h-PDMS material was spin coated on either the FDTS coated master or on the thin glass sheet on top of the stamp configuration. After this, the master and the thin glass were put in contact and the system was kept in vacuum chamber to eliminate all air bubbles in between the master and the glass sheet. Fi-

nally the h-PDMS stamp was cured on a hotplate at 80 °C for at least an hour. The cured stamp and the master were carefully separated and the master was washed with Pana-solve-solution (2:1 mixture of dichloromethane and Lutensit A-LBS cleaner solution) to remove the PDMS remnants, after which it can be used again to fabricate new stamps.

5.4.2 The chemistry of microcontact printing process

The silane compound used for microcontact printing is (3-mercaptopropyl)trimethoxysilane (MPTMS) that has an thiol group at one end of the molecule and a trimethoxysilane group at the other end (Figure 5.7). The substrates are either silicon wafers with thin native oxide layer, silicon wafers onto which 30 nm thick layer of silica (SiO_2) is grown by PECVD or microscope glass slides, which are actually also made of silica.

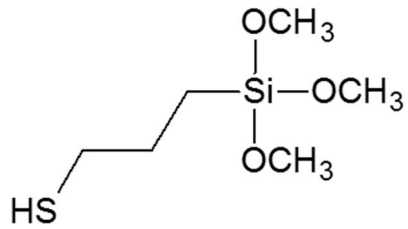

Figure 5.7. *(3-Mercaptopropyl)trimethoxysilane (MPTMS), the molecule used for microcontact printing.*

The driving force for the self-assembly of alkylsilanes on top of silicon substrates is in situ formation of polysiloxane, which is connected to surface silanol groups (-SiOH) via Si-O-Si bonds. [92] To create the required surface silanol (Si-OH) groups on the substrate surface, the substrates were cleaned in hot piranha solution (4:1 H_2SO_4 and H_2O_2) followed by oxygen plasma activation, just like in the block copolymer process (Chapter 5.2). These silanol groups are vital for the attachment of MPTMS molecules, which takes place via covalent Si-O-Si bonds between the silanol groups on the substrate surface and the trimethoxysilane groups in MPTMS as shown in Figure 5.8. [92]

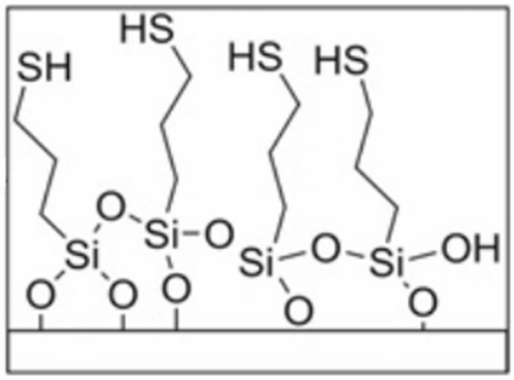

Figure 5.8. *Attachment of MPTMS onto activated silicon surface. The attachment takes place in the trimethoxysilane end of an MPTMS molecule so that the thiol groups point outwards.*

MPTMS molecules form a self-assembled monolayer (SAM) on top of the silica surface. The reproducibility of alkylsilane monolayers can be difficult due to the self-polymerization reaction in solution that may result in significant difference in SAM quality. [92] The prospect of polymerization was reduced by preparing a new MPTMS solution for each microcontact printing.

The inking of the stamps with MPTMS was achieved by a contact inking method [93]. A piece of s-PDMS mattress was cut to suitable size and dipped into 5 mM MPTMS solution in ethanol for more than 12 hours. After that, the PDMS mattress was blown dry with N_2 stream and stored in a glass flask and used within 3 hours. The stamp prepared earlier was put in contact with the inked PDMS mattress without applying pressure for 40 s and then stamped using the microcontact printing process.

5.5 Quantum dot deposition

The quantum dots used in this thesis are colloidal quantum dots purchased from CanDot Inc. Their core is cadmium selenide (CdSe), the shell cadmium sulphide (CdS) and the ligand is oleylamine (Figure 5.9).

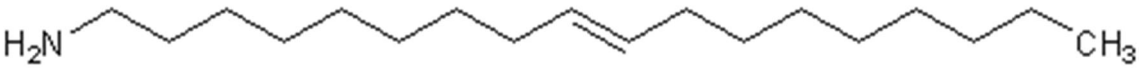

Figure 5.9. *Oleylamine, the ligand in the CdSe/CsS quantum dots used in this thesis.*

The ligand is bound to the CdS shell by electrostatic forces which are not very strong. The idea for the attachment of QDs to MPTMS layer on top of the silicon substrate is that the thiol groups in MPTMS would form a stronger, covalent bond with the QD shell and hereby replaces the oleylamine ligands. When the MPTMS is selectively stamped on some areas of a silicon wafer, the quantum dots would only bind to the outwards-pointing SH-groups in MPTMS and thus selective deposition of QDs would be achieved.

The deposition of quantum dots on MPTMS covered silicon surfaces was attempted by dipping the samples in dilute QD solutions in hexane for 6 hours. The concentrations of the solutions varied between $8{,}0\times10^{-5}$ to $2{,}5\times10^{-4}$ mol/l.

5.6 Other measurement methods

Besides the measurement methods presented earlier, a number of other scientific research equipment was used. Different kinds of microscopy techniques have to be applied when working with samples with dimensions in the micro- or nanoscale. Scanning electron microscopy, atomic force microscopy and fluorescence lifetime microscopy are imaging techniques for mico- and nanoscale pattern detection and the basic principles of these three methods are described in this chapter.

5.6.1 Scanning electron microscopy

Scanning electron microscopy produces images by scanning a beam of electrons on top of the surface of a substrate as in e-beam lithography described in Chapter 3.1. The detected electrons are usually secondary electrons emitted from the surface and the detection of these electrons generates the image of the structural details of the surface. The imaging is done under ultrahigh vacuum and the incident beam energy can be as high as 30 keV. Depending on the energy of the electron they can penetrate the surface to about the depth of 1 µm. A schematic drawing of SEM equipment is presented in Figure 5.10.

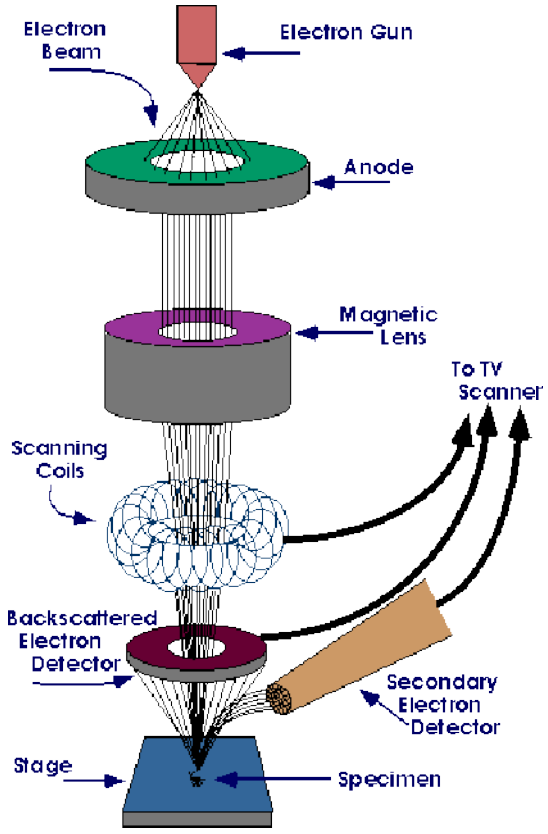

Figure 5.10. *Schematic drawing of a scanning electron microscope (SEM). [94]*

At the top of the microscope lies the electron gun that is used to produce the electron beam. The beam is directed vertically through the microscope, where it travels through several lenses and electromagnetic fields, which focus the beam toward the sample. When the beam hits the sample, electrons and X-rays are ejected from the surfaces. Detector collects the backscattered electrons and secondary electrons and convert them into a signal and finally into an image of the surface under study.

Only conductive samples can be measured with SEM. Therefore, all insulating-samples have to be covered with a thin layer of some conductive material or the electron beam induced charging of the surface must be compensated e.g. by injecting ions with an opposite charge. [94], [95] The SEM instrument used in this thesis was Carl Zeiss SMT SEM Ultra-55 scanning electron microscope.

5.6.2 Atomic force microscopy

Atomic force microscope (AFM) belongs to a group of instruments called scanning probe microscopes (SPMs). The common factor in all SPM techniques is the use of a very sharp probe, which is scanned across a surface of interest to produce a high resolution image with the interactions between the probe and the sample. This way, the AFM instrument can build a detailed image of the topography and texture of the sample material. The schematic structure of an AFM instrument is shown in Figure 5.11.

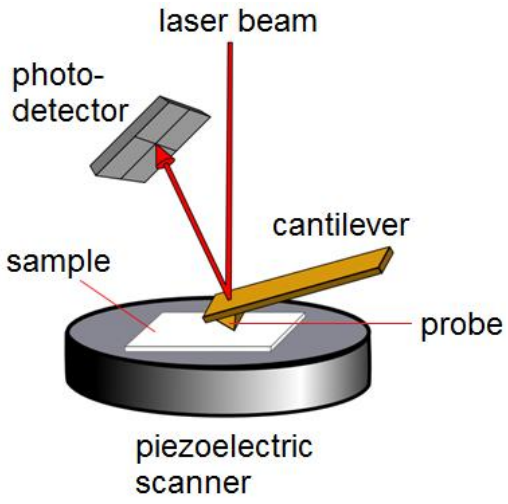

Figure 5.11. *Basic AFM set up consisting of a cantilever with the probe attached to its end, a piezoelectric scanner to move the probe in relation to the sample surface and a photodetector to monitor the deflections of the cantilever via a laser beam reflected to the detector through the cantilever.*

The AFM instrument consists of a sharp probe mounted near to the end of a flexible microcantilever arm. Either the cantilever itself or the sample surface is mounted on a piezocrystal which allows the position of the probe to be moved in relation to the surface. The cantilever is lowered to touch the surface of the sample and the sample surface is raster scanned. A beam of laser light is refected from the upper side of the cantilever onto a position-sensitive photodetector. Any defection of the cantilever will produce a change in the position of the laser spot on the photodetector, allowing changes to the defection to be monitored. The microscope stage is usually supported on a vibration isolation platform to reduce any disturbance. Besides the microscope stage itself, the AFM machinery contains the control electronics and a computer to operate the system. [96], [97]

AFM measurements in this thesis were carried out with Veeco Dimension 3100 atomic force microscope in the tapping mode and the tips used were Nanosensors^{TM} point probe plus tapping tips (model PPP-NCH-50).

5.6.3 Fluorescence lifetime microscopy

Fluorescence lifetime microscopy (FLM) is based on the fluorescence emission from a sample to be studied. The images in FLM are produced based on the differences in the decay rate of the fluorescence from a fluorescent sample. Figure 5.12 shows a schematic drawing of a FLM instrument. An excitation light is illuminated towards the sample and its emission radiation is gathered in the detector. A CCD (charge-coupled device) camera monitors the quality of the focus by detecting the backscattered and –reflected excitation light from the objective. Exitation power is monitored by the photodiode (PD) during the measurements. Two shutters in the excitation beam path and in front of the detector ensure safe operation. A pinhole situated in the intermediate image plane, acts as a spatial filter and allows only the in-focus portion of the light to be detected. [98]

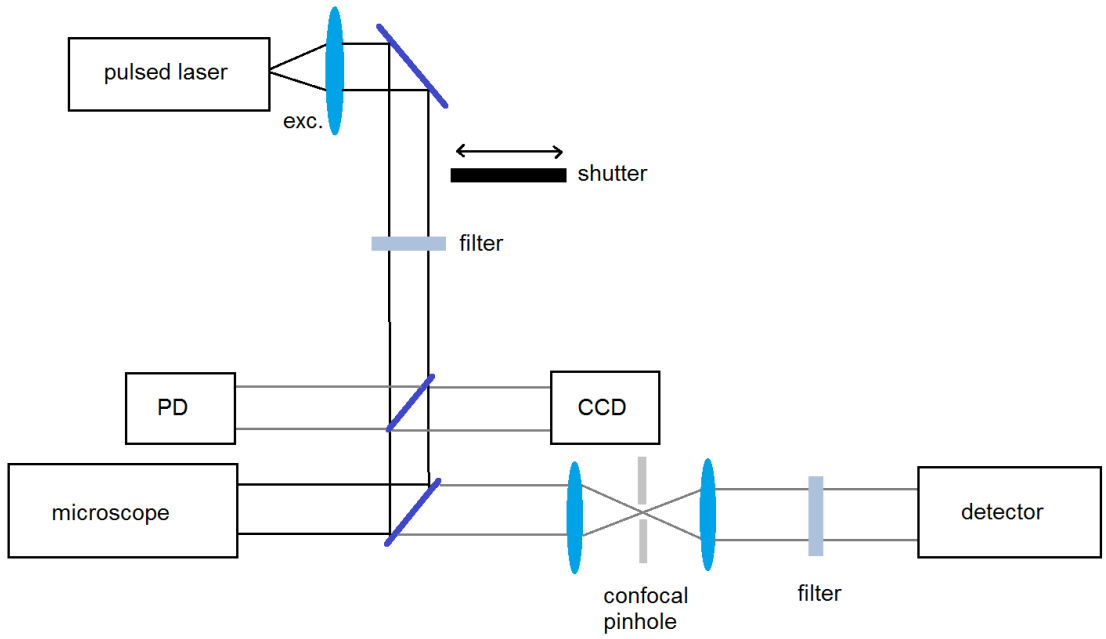

Figure 5.12. *Schematic drawing of a fluorescent lifetime microscope. PD stands for the photodiode and CCD for the charge-coupled device. [98]*

Fluorescence lifetime images in this Thesis were acquired by an inverse time-resolved fluorescence microscope, MicroTime-200 coupled with an Olympus IX71 microscope (PicoQuant GmbH). The excitation wavelength, the spatial resolution, and the time resolution were 405 nm, 0.3 µm, and 60 - 70 ps, respectively. The manufacturer's software was used to analyze the data and calculate the lifetime maps.

The fluorescent probe used to study the attachment of stamped MPTMS molecules on substrates was monobromobimane (mBBr). While mBBr itself is nonfluorescent, it alkylates the thiol groups in MPTMS molecules displacing the bromine in mBBr and thus adding the fluorescent tag to the thiol. The wavelength of the fluorescent emission of this compound is 478 nm. [99] After the microcontact printing of MPTMS, the substrates were dipped into 10mM mBBr solution in acetonitrile for >12 hours after which they were rinsed with the solvent and then measured with FLM.

6 RESULTS AND DISCUSSION

This chapter summarizes the results of the experiments. The results of the block copolymer self-assembly on both non-patterned and patterned substrates are presented and the differences between the different block copolymer mixtures and the effect of the underlying substrate on the assembly are discussed. Trench and square well patterns of different dimensions were applied in topographical patterning process and these results are represented here with discussion about the etch depth effect on the quality of the pattern. SEM images of the masters fabricated by transferring the self-assembled block copolymer pattern into the underlying substrate are shown as well as the results of NIL process using these stamps. Finally, the results from microcontact printing process with MPTMS are shown and the problems faced with microcontact printing are discussed.

6.1 Block copolymer self-assembly on non-patterned substrates

Figure 6.1 represents the results of the self-assembly of two different compositions of PS-*b*-PMMA block copolymers on silicon substates pretreated with a hydroxyl terminated PS-*r*-PMMA random copolymer brush to obtain surface perpendicular PMMA cylinders. The samples were fabricated according to the process in Appendix 1.

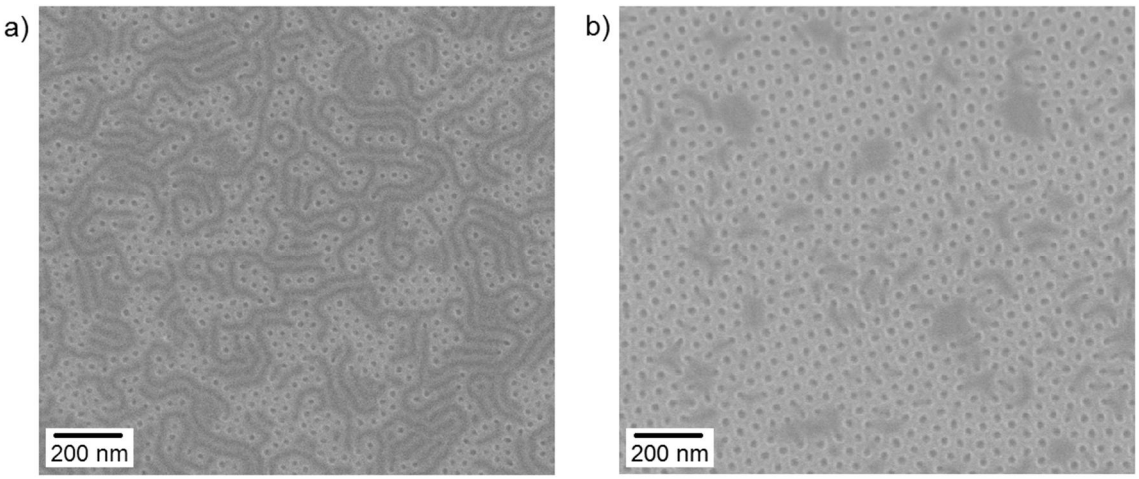

Figure 6.1. *SEM images of block copolymers P(67.1)-SMMA (left) and P(101.5)-SMMA (right) assembled on silicon surface. PMMA cylinders are already etched off by reactive ion etching.*

It is clear from the Figure 6.1 that the assembly of polymer P(67.1)-SMMA (Figure 6.1a) is much less organized than that of polymer P(101.5)-SMMA (Figure 6.1b). In

Figure 6.1a about half of the cylinders are organized in a substrate parallel manner that is a common behavior for PS-*b*-PMMA block copolymers in the absence of surface neutralizing layer. This indicates that the underlying surface neutralizing PS-*r*-PMMA monolayer might not cover the whole substrate surface sufficiently well to form a neutral underlayer. P(101.5)-SMMA polymer in Figure 6.1b, on the other hand, does not show this kind of behavior but all the cylinders are assembled in surface perpendicular manner. However, there are a number of defects in the template that could also be due to an imperfect imaging layer.

To investigate the effect of the substrate surface on the self-assembly process, another experiment was carried out by applying a 30 nm thick layer of SiO_2 on top of similar silicon substrates used earlier. The results for both polymer compositions are shown in Figure 6.2.

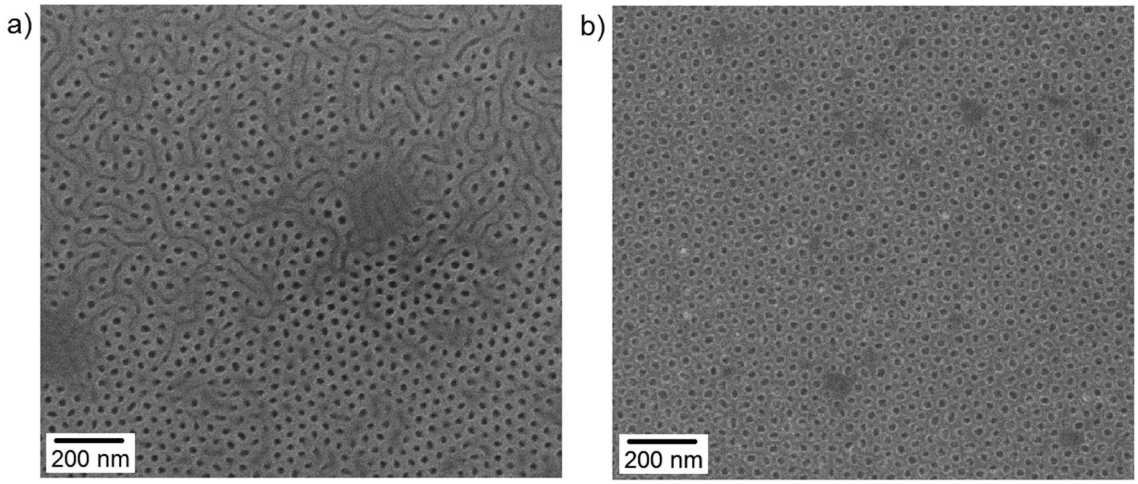

Figure 6.2. *SEM image of block copolymers P(67,1)-SMMA and P(101,5)-SMMA assembled on silicon surface with a 30 nm thick SiO_2 layer. PMMA cylinders are already etched off by reactive ion etching.*

Both polymer templates still show some defects but overall the assembly is much better compared to the samples in the Figure 6.1. From this experience, it can be said that the native oxide layer on the silicon substrates is not sufficient to produce surface silanol groups with the treatments used here (piranha clean and oxygen plasma treatment). Silanol groups act as the attachment sites for the hydroxyl-terminated PS-*r*-PMMA block copolymer molecules and in the absence of these groups, the attachment of the surface neutralizing PS-*r*-PMMA layer to the substrate surface is incomplete. When using SiO_2 covered substrates, the formation of silanol groups is more efficient possibly due to the increased amount of oxygen on the surface. With more silanol groups, the quality of the surface neutralizing random copolymer layer becomes much better.

For some reason, the assembly of block copolymer P(101.5-SMMA) (Figures 6.1b and 6.2b) is more organized than the assembly of block copolymer P(67.1)-SMMA (Figures 6.1a and 6.2a) no matter which substrate is used. The exact reason for this is unknown but as only one sample ordered from Polymer Source was used, there is a pos-

sibility that the quality of the polymer sample was not uniform. After this observation, most of the experiments were conducted using polymer P(101.5)-SMMA.

6.2 Directed self-assembly on patterned substrates

Topographical patterns of trenches in widths of 90 - 180 nm were patterned on silicon substrates by electron beam lithography as explained in Chapter 5.3.1. The patterns were etched into silicon to the depth of 35 or 50 nm as revealed by atomic force microscopy (Figure 6.3). The depth of 35 nm was achieved after 6 seconds of etching while the 50 nm depth required 8 seconds. Figure 6.4 represents a 3D image of the substrate surface after the patterning.

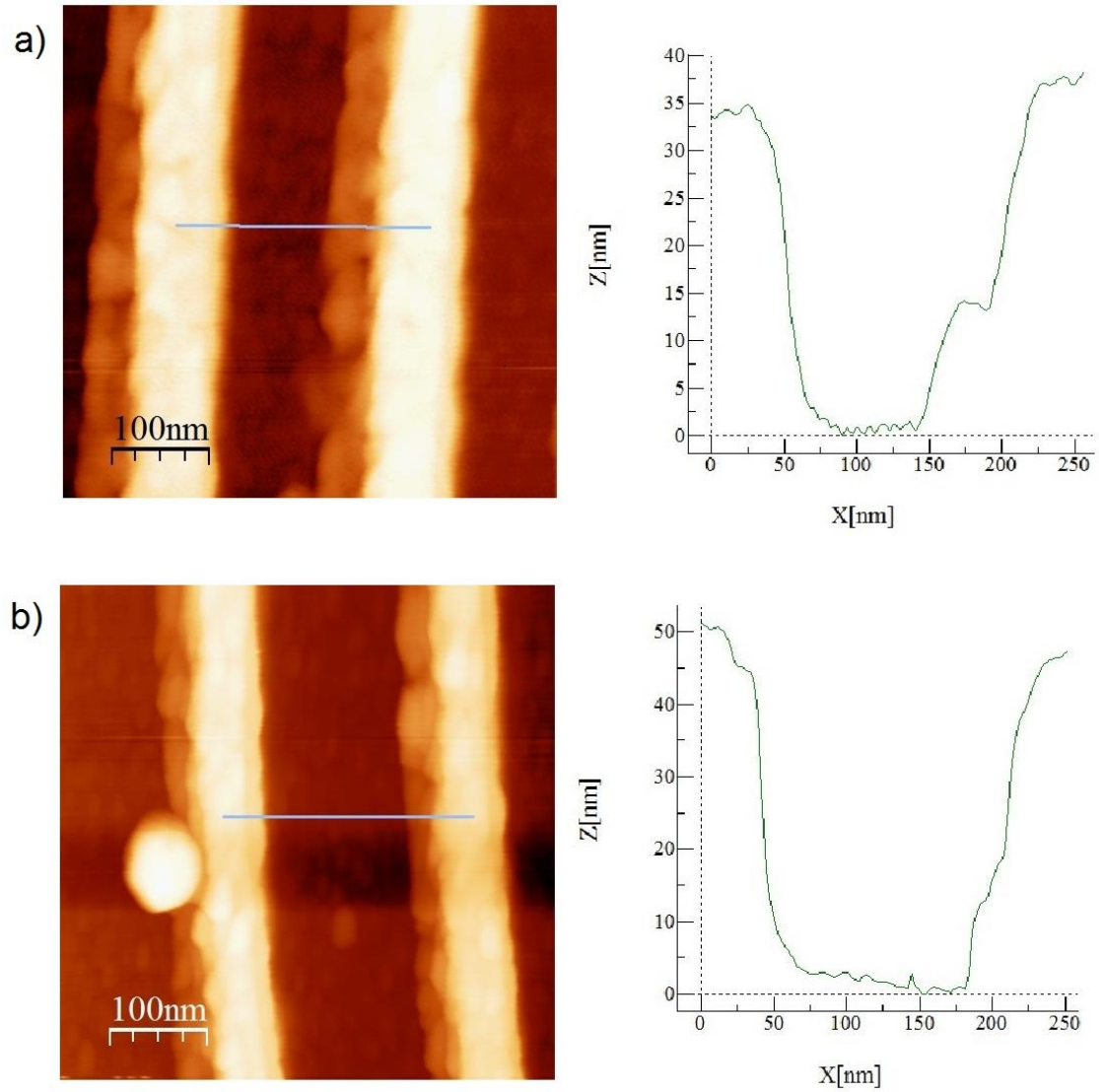

Figure 6.3. *AFM image (left)and the cross-section diagram (right) of a topographically patterned trench structure etched in silicon with RIE for a) 6 seconds and b) 8 seconds resulting in 35 and 50 nm deep trenches, respectively. The vertical line in the AFM image shows the location of the cross-section.*

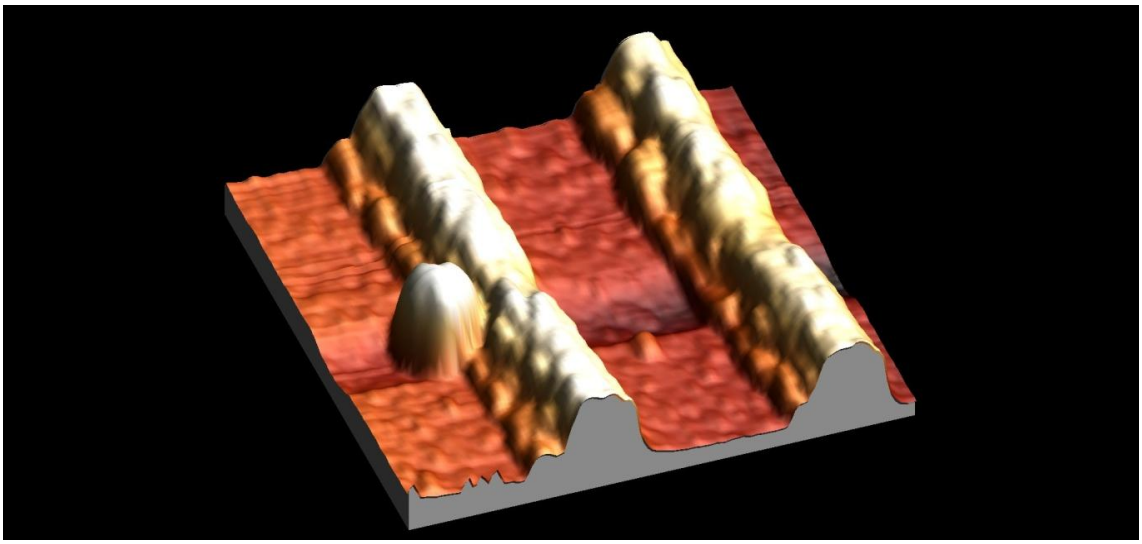

Figure 6.4. *An AFM 3D presentation of the 50 nm deep topographical trench pattern etched in silicon.*

The bulge on the left side of the trenches visible in all of the AFM images is most probably due to a disruption in the AFM scanning tip and not really present in the samples. After the etching, a thin, 10 nm layer of silica was applied on top of the substrates, thus making the patterns a little lower and thinner. After this the surface neutralizing random BCP layer and then the PS-*b*-PMMA block copolymer layer were annealed on top of the patterned substrate. Figure 6.5 represents the SEM images taken from the samples with block copolymer P(67.1)-SMMA and Figure 6.6 those of the samples with block copolymer P(101.5)-SMMA annealed on top of the trench pattern. Both polymers were annealed on both 35 and 50 nm deep trench patterns.

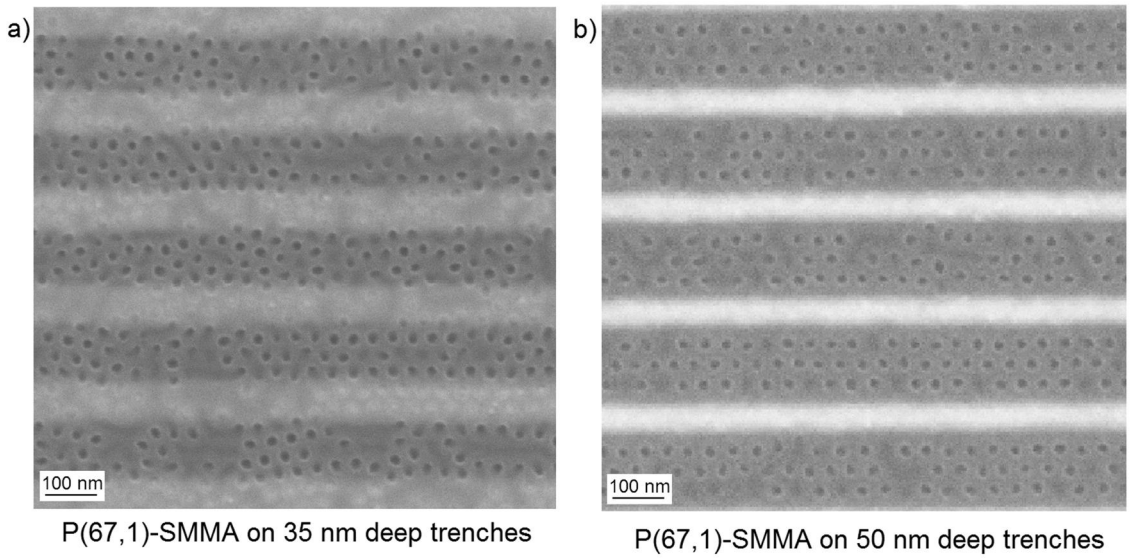

Figure 6.5. *SEM image of P(67.1)-SMMA block copolymer annealed on top of the a) 35 nm and b) 50 nm deep trenches.*

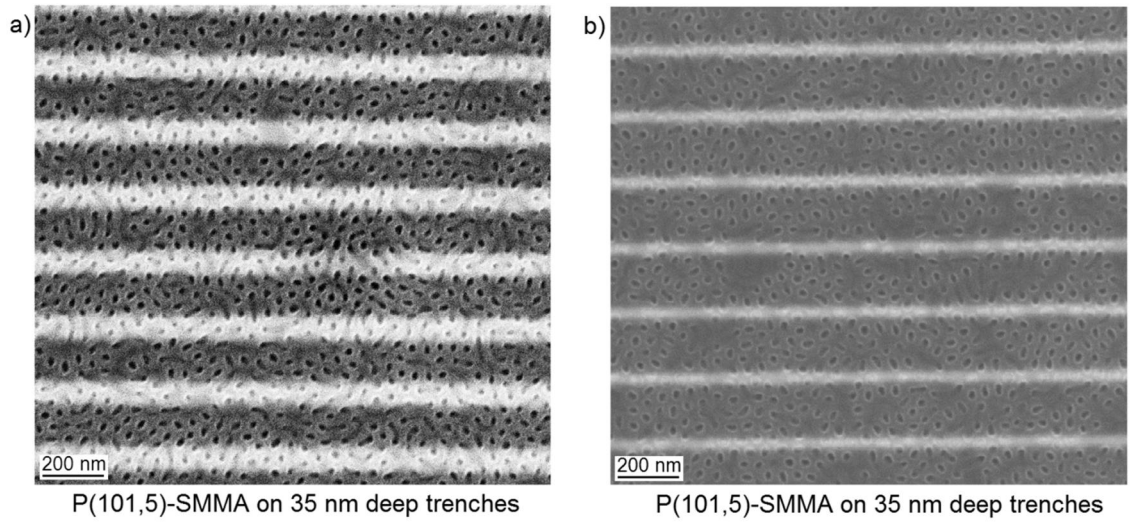

Kuva 6.6. *SEM image of P(101.5)-SMMA block copolymer annealed on top of the a) 35 nm and b) 50 nm deep trenches. SEM image of P(67,1)-SMMA block copolymer annealed on top of the a) 35 nm and b) 50 nm deep trenches.*

The patterns written by electron beam lithography always appear a little wider than written due to the electron backscattering and imperfect focus of the beam. The etching process also broadens the patterns. Then again, the SiO_2 layer applied on top of the pattern narrows them a bit. The patterned trench width as written with EBL in Figure 6.5 was 115 nm but the resulting trench widths measured from the SEM images were approximately 115 nm (6.5a) and 140 nm (6.5b). Similarly, the EBL trench width in Figure 6.6 was 130 nm but the resulting trench widths were 130 nm (6.8a) and 180 nm (6.8b). The longer etch time broadens the patterns with tens of nanometers and this should be taken into account when designing the prepatterns for block copolymer lithography. Unfortunately, the PMMA e-beam resist used here is really sensitive to any changes in the EBL process and exactly similar results are difficult to obtain for each writing process.

As can be noted by comparing a) and b) sections of each of the Figures 6.5 and 6.6, the results are much better on the deeper, 50 nm trench pattern. The polymer layer annealed on top of the substrate is approximately 30 nm deep as revealed by ellipsometry measurements and 35 nm deep etch patterns do not seem to be deep enough to guide the self-assembly process. In Figure 6.6a the polymer domains even reach the top of the trenches and “slide” down to the bottom resulting in elongated cylindrical structures at the edges of the trenches.

When comparing Figures 6.5b and 6.6b with each other, one unexpected result is observed. Even though the self-assembly of polymer P(101.5)-SMMA was remarkably better on unpatterned surfaces than that of polymer P(67.1)-SMMA, on patterned surfaces here, the smaller molecular weight polymer P(67.1)-SMMA forms much more organized structures (Fig 6.5b). The samples were prepared at the same time so there is no deviation in the samples and the only difference is the polymer used. This observation must be due to the BCP pattern directing characteristic resulting from the confine-

ment of the walls. It has been noted earlier that guiding patterns rectify the dislocations in self-assembled BCP patterns [62] and in this case the surface parallel cylinders that were present on nonpatterned substrates have vanished due to the strong confinement that forces all the cylinders to align in substrate perpendicular orientation. The reason the confinement does not effect as strongly in P(101.5)-SMMA block copolymer is unclear.

The AFM image with a cross section profile diagram of P(67.1)-SMMA annealed on top of 50 nm deep trench patterns is shown in Figure 6.7 and the 3D image of the surface in Figure 6.8.

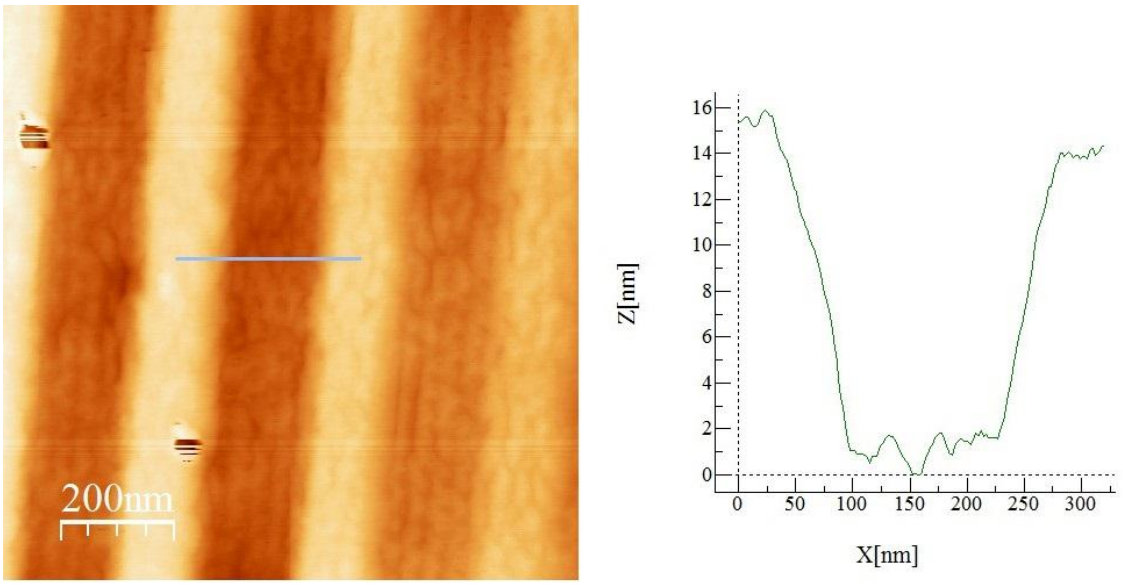

Kuva 6.7. *AFM image (left) and the cross-section diagram (right) of a 50 nm deep topographical trench pattern with the P(67.1)-SMMA polymer annealed on top. PMMA domains are already etched off.*

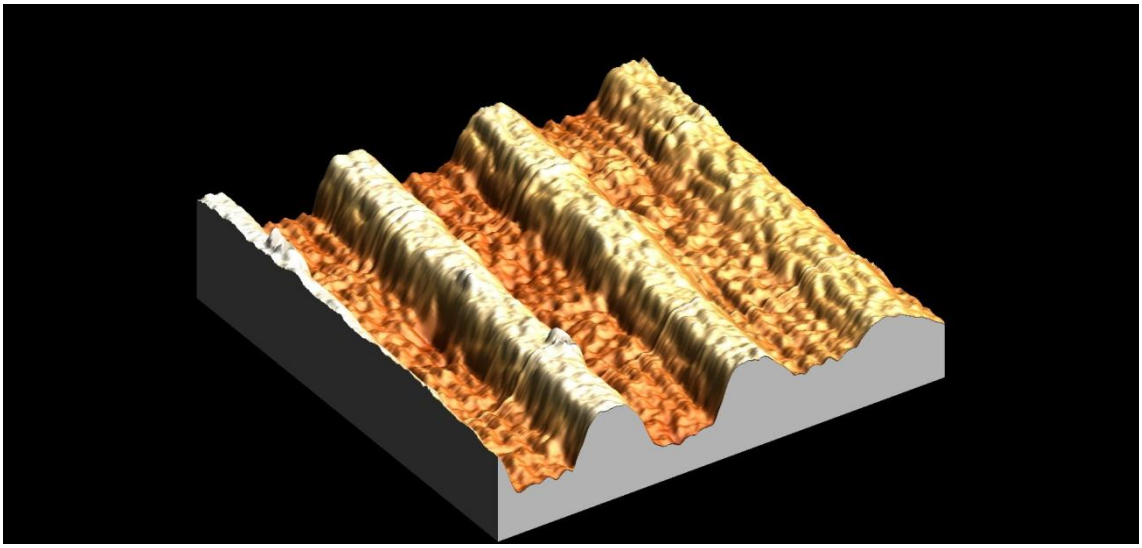

Kuva 6.8. *An AFM 3D presentation of the 50 nm deep topographical trench pattern with the P(67.1)-SMMA polymer annealed on top. PMMA domains are already etched off.*

The AFM images show how the applying of the block copolymers on top of the trench pattern has changed the surface topography of the sample. The AFM tip is not small enough to penetrate the small nanoholes formed by the etching of the PMMA cylinders to get the full depth profile but nonetheless the surface structure is clearly visible in both Figures 6.7 and 6.8. It can be seen from the cross section image in Figure 6.7 that the depth of the trenches has lowered from 50 to 16 nanometers after applying the block copolymer layer. The thickness of the block copolymer layers as measured by ellipsometry is approximately 30 nm so it can be concluded that the polymer layer is packed mostly at the bottom of the trenches and not on top of the mesas.

Another set of topographical patterns were also prepared by fabricating lines of gold to form the sidewalls of the trench pattern on top of a surface neutralizing random layer. The gold sidewalls were obtained by a lift-off process described in Chapter 5.3.1 and in Appendix 3. The dimensions of the trenches varied between 90 – 180 nm. Figure 6.9 depicts both block copolymer mixtures annealed on top of 50 nm deep gold trenches.

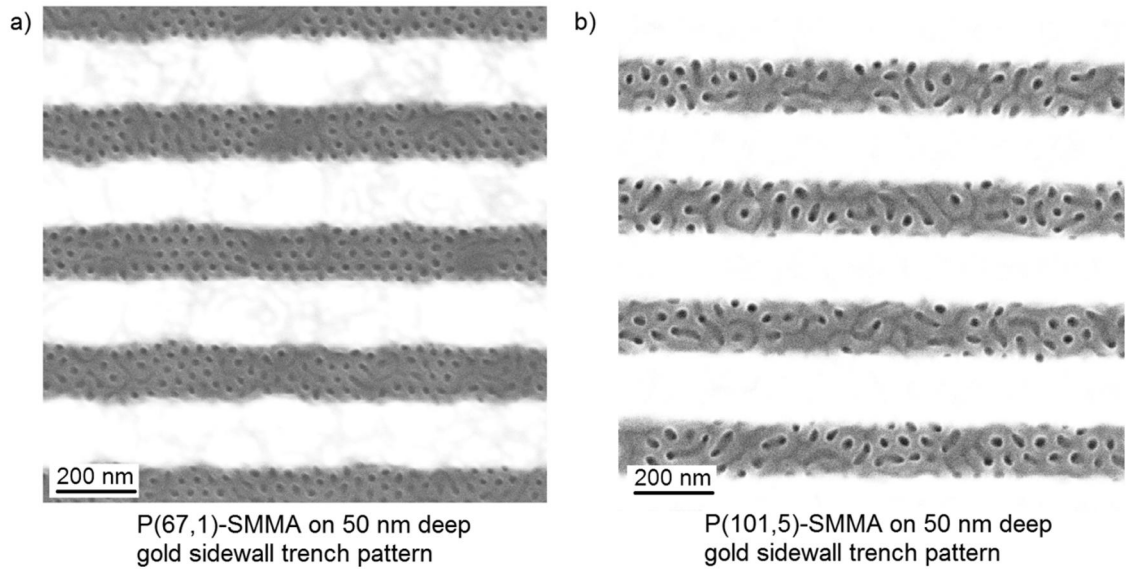

Kuva 6.9. *SEM image of a) P(67.1)-SMMA block copolymer and b) P(101.5)-SMMA block copolymer annealed on top of 50 nm deep trenches with gold sidewalls and neutral bottom. The designed width of the patterned trench was 175 nm but the resulting trenches are ~144 nm wide.*

Once again, the arrangement of P(67,5)-SMMA polymer is more ordered than that of P(101,5)-SMMA polymer. However, the gold sidewalls did not improve the organization of the BCP domains as can be seen when comparing Figures 6.5b and 6.9a.

In addition to the trench patterns, square wells with dimensions of 50 – 120 nm were topographically patterned on the substrates. The process is described in Chapter 5.3.1. The difference between the square wells and trench patterns is that there is no surface neutralizing random copolymer layer in square well patterns but the surface perpendicular alignment of the cylinders is obtained due to the strong confinement effect from the walls of the patterns. The square wells patterned by EBL were etched into silicon down to a depth of 60 nm (Figure 6.10) to ensure that the depth of the patterns is higher than that of the polymer layer.

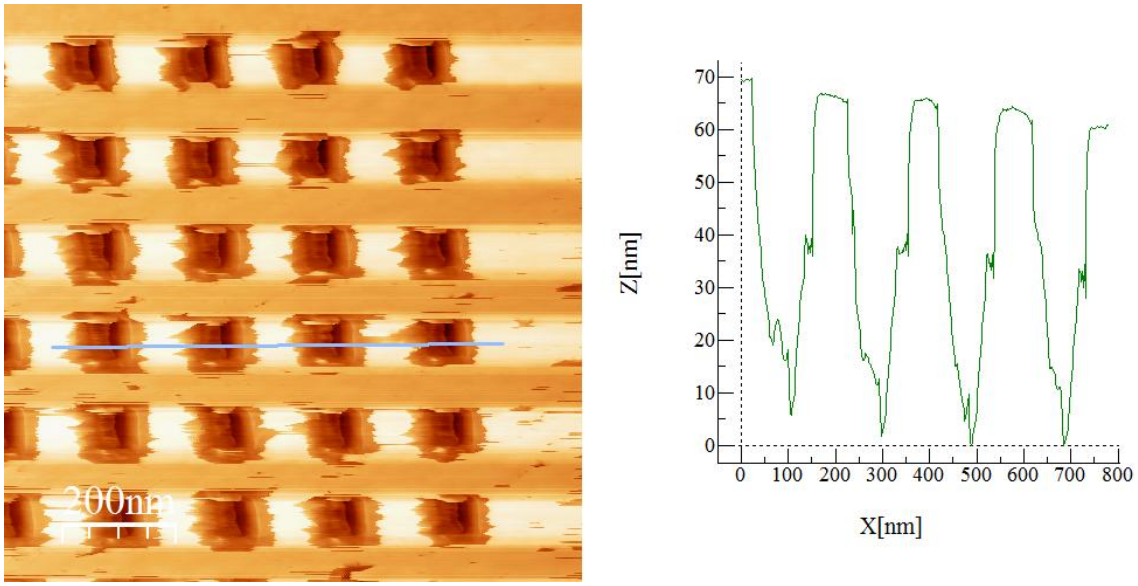

Kuva 6.10. *AFM image (left) and a cross section (right) of square well patterning template etched in silicon. The blue line in AFM image shows the location of the cross-section.*

Again, the AFM image shows that the tip is not completely in order but the depth of the features can still be observed. Both block copolymers were annealed on top of the square well patterns but this time P(67.1)-SMMA showed almost no ordered arrangement. The problem can be in the polymer solution. New solutions for each of the block copolymers were prepared for this experiment and as noted earlier, it seems like there might be some variation in the quality of the polymer and this is probably why different solutions of the same polymer sometimes gave very different results. The experiments should probably be repeated several times with always a new polymer solution but in the scope of this thesis it was not possible since the annealing process is so time consuming (up to 5 days for most of the processes). Figure 6.11 represents the poor square well results for P(67.1)-SMMA block copolymer and figure 6.12 the results for P(101.5)-SMMA block copolymer in four different sizes of the square wells.

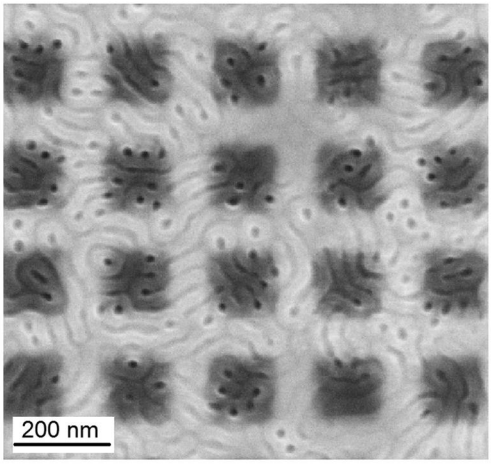

square side length 70 nm

Figure 6.11. *SEM iamges of block copolymer P(67.1)-SMMA annealed on top of square well topographical patterns with side length of 70 nm.*

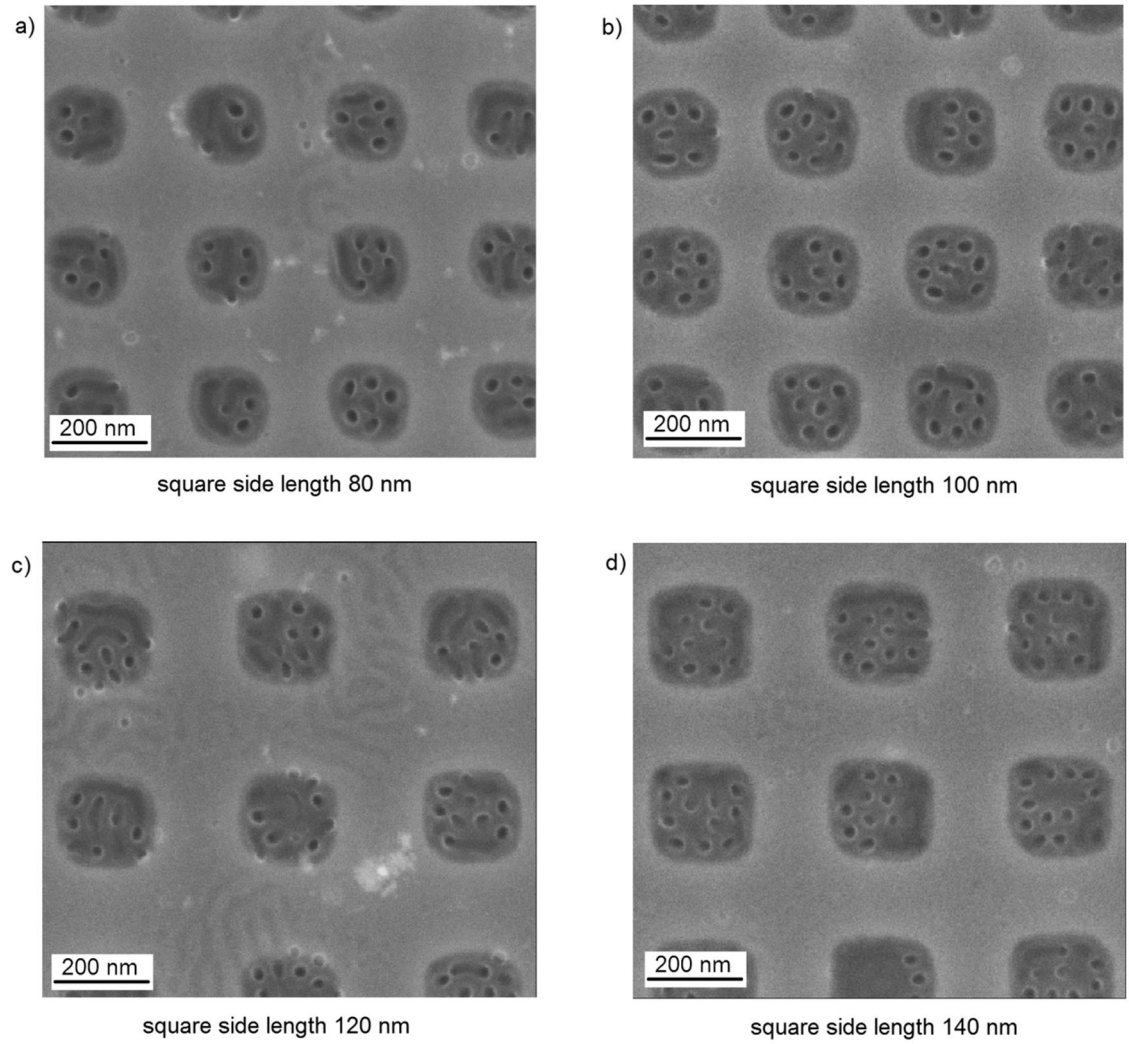

square side length 80 nm

square side length 100 nm

square side length 120 nm

square side length 140 nm

Figure 6.12. *SEM images of block copolymer P(101.5)-SMMA annealed on top of square well topographical patterns of different dimensions. The square side lengths below the images are the designed lengths. The actual side lengths after silicon etching are about 70 nm longer than designed.*

It can be seen from the SEM images in Figure 6.12 that the cylinders of PMMA do indeed arrange inside the square wells in surface perpendicular fashion but once again, the alignment is not perfect and uniform but there are defects and dislocations. To achieve a better alignment, the corners of the e-beam prepatterned squares should be much sharper. Now they round up a lot, which makes the confinement effect less strong. In addition, arrangement of the cylinders in a square is not natural for the block copolymer as they prefer the hexagonal arrangement to minimize the repulsion energy. Thus, a hexagonal or a triangular prepattern could work better.

6.3 Stamp fabrication from block copolymer templates

Masters for stamp preparation were fabricated from annealed block copolymer samples by first removing the cylindrical PMMA domains and then applying different dry etching methods to transfer the nanohole pattern onto the underlying substrate. In some cases the etching was done by using only the remaining polystyrene layer as an etch mask while in other cases a 5 nm thick layer of chromium was evaporated on top of the pattern in a 45° angle to avoid deposition of chromium on the bottom of the holes. Table 6.1 lists all the prepared masters, the substrates and the etching parameters.

Table 6.1. *Prepared masters. The first number in the master number indicates the underlying substrate (1 = Silicon, 2 = Silicon + SiO_2) and the second one the variation in etching conditions.*

Master number	Surface	Etch gases	Etch time (s)
1.0	Si	SF_6 and O_2	5
2.0	Si + 30 nm SiO_2	SF_6	40
2.1	Si + 30 nm SiO_2	CHF_3 and O_2	80
2.2	Si + 30 nm SiO_2 + 5nm Cr mask	CHF_3 and O_2	80

Silicon substrate without the silica layer was used in only one of the samples because, as noted before, the ordering of the BCP domains is much better if there is a layer of SiO_2 on top of the substrate. The etching parameters were evaluated from the previous etching experience at ORC as well as from scientific articles [8]. The SEM images of the masters obtained by etching and removing the remaining polystyrene are shown in Figure 6.13.

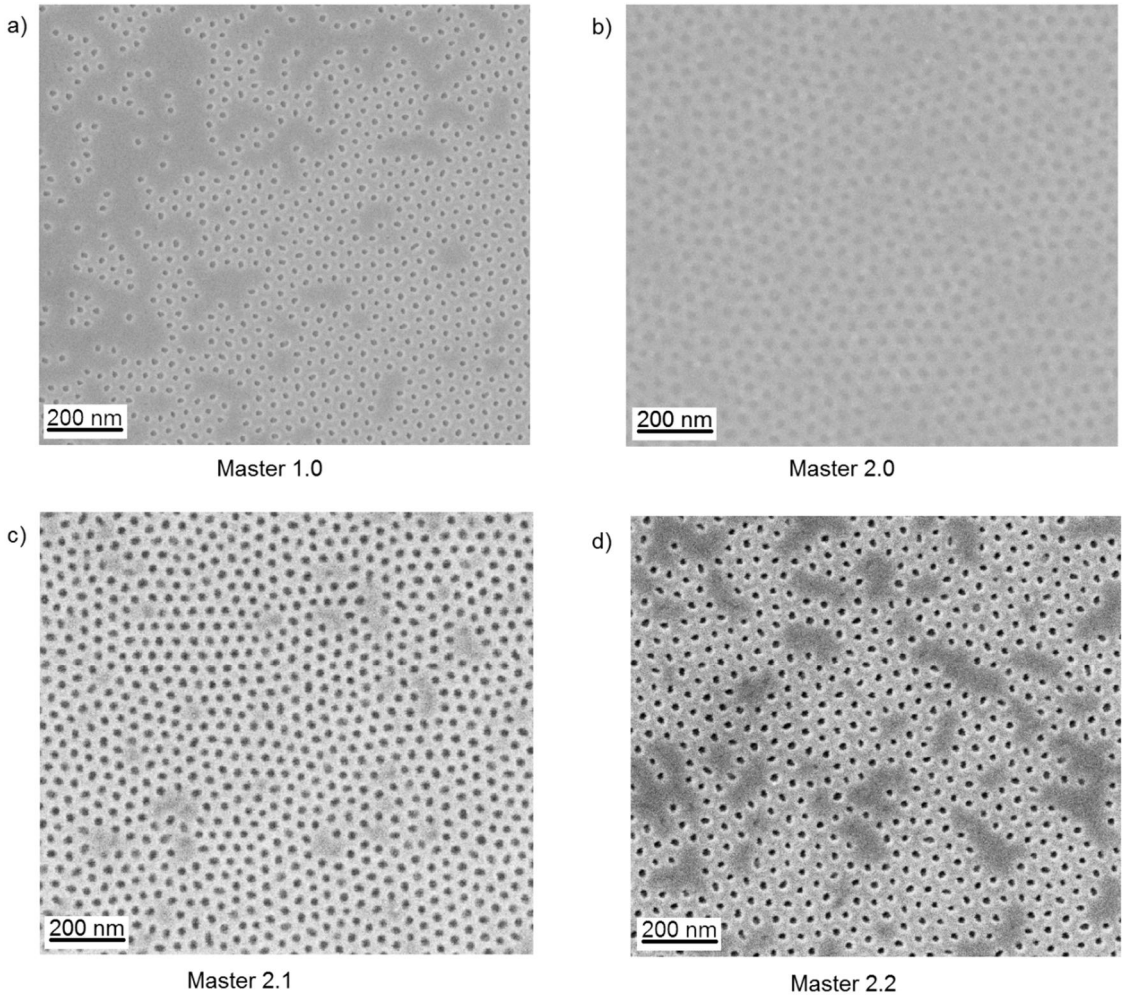

Figure 6.13. *SEM images of the masters prepared for stamp fabrication.*

It is visible from Figure 6.13a that the assembly of the BCP domains has once again been imperfect on a silicon substrate (master 1.0). Better assembly was achieved near some defects like small pieces of debris on the sample surface. This is the case in the lower right corner of figure 6.13a. The etching seems to be quite low judging from the low contrast in the SEM image.

Two different etching processes were applied on the silica covered surfaces. The contrast in Figure 6.13b is low which indicates that the SF_6 etch is not efficient and does not produce deep enough patterns. However, CHF_3/O_2 etch seems to work really well both on the surfaces etched with and without a chromium etch mask. The pattern has been transferred to the underlying substrate pretty much as it is and the etch depth seems deeper than in the first two images. The contrast in the SEM image really gives only an indication about the depth of the features. AFM or a cross section SEM image would be better methods to study the depth profile, but here the small dimensions of the features make the application of these methods extremely difficult.

Elastomeric h-PDMS stamps were made using all the masters shown in Figure 6.13. The patterns on the prepared stamps themselves cannot be viewed as the dimen-

sions are too small for optical microscopes (tens of nanometers) and SEM imaging would require applying a conductive layer on top of the stamp. This was attempted by evaporating a thin layer of gold on top of the stamp, but it turned out that the metal flakes covered the small surface relief patterns altogether. Thus, the method for evaluating the stamps was to perform a nanoimprint lithography (NIL) process, where a photoresist is spread on top of a substrate and the stamp and the substrate are pressed together so that the resist adjusts to the stamp relief patterns. Then the resist is cured with UV light and finally the stamp and the substrate are separated carefully. Normally the printed pattern on the resist would be etched to transfer the pattern to the underlying substrate but in this case suitable etch parameters proved difficult to find and all the etching attempts led to vanishing of any features. SEM images of the stamp patterns transferred to resist layer by NIL are shown in Figure 6.14.

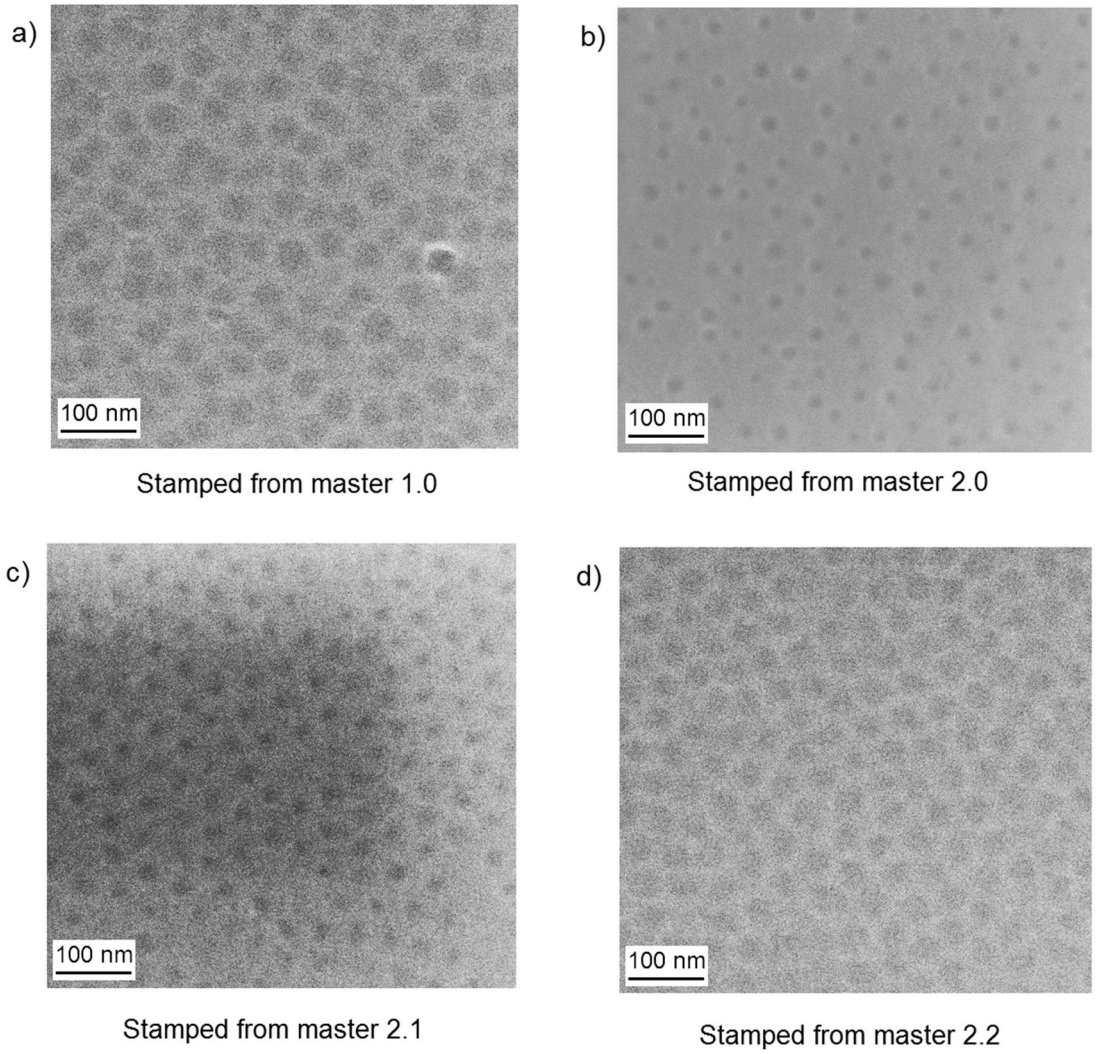

Figure 6.14. *SEM images of patterns printed by nanoimprint lithography on mrUV-cur resist with stamps made from masters 1.0 - 2.2.*

The dimensions of the patterns have somewhat widened during the stamp making process. The NIL patterns produced with the stamps made from masters 1.0 and 2.1 display

more defects and sparse patterns. On the contrary, the stamped patterns masters 2.1 and 2.2 (Figure 6.14c and 6.14d) seem to be the most successful in transferring the nanopattern through NIL process as could be expected due to the better master quality. However, the fact that all the SEM images have such low contrast and that the patterns could not be etched point towards the fact that the depth of the features in the stamp is really low. This can either be due to the fact that the patterns in the master are already really low or then the h-PDMS stamp material does not fill the holes completely but curves to the sides of the hole and leaves the bottom untouched.

6.4 Microcontact printing

Microcontact printing process was first carried out using a flat s-PDMS mattress without any relief patterns as a stamp to study the attachment of MPTMS on the substrates. After the printing, substrates were dipped in fluorescent probe solution to induce fluorescent emission in MPTMS covered areas of the samples. The studied substrates were silicon, silicon substrate with 30 nm SiO_2 coating and microscope glass (Figure 6.15).

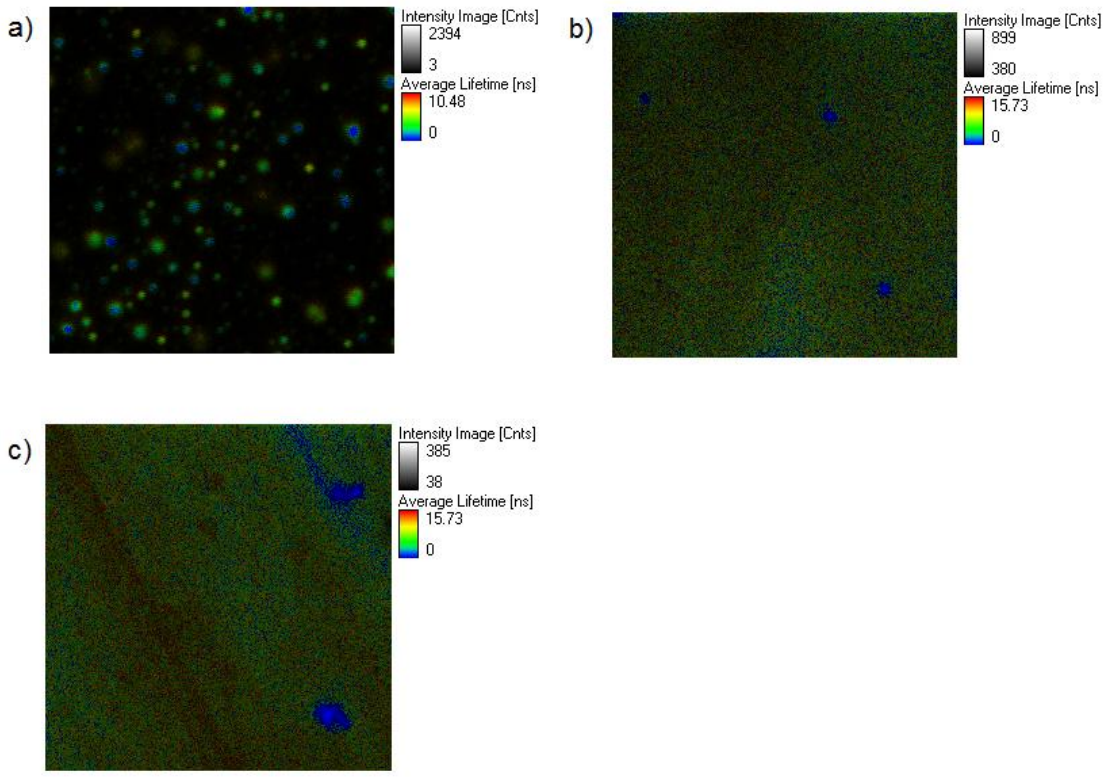

Figure 6.15. *Fluorescence lifetime microscopy images of a) silicon b) silicon with 30 nm SiO_2 and c) microscope glass substrates onto which MPTMS stamped with a flat, unpatterned stamp. The color scales represent average lifetime, and the total number of counts is indicated by color density at each point. The dimensions of each image are 40×40 µm.*

Figure 6.15 shows clearly that the attachment of MPTMS molecules on silica (6.15b) and microscope glass (6.15c) surfaces is much better than on silicon surface (6.15a).

This observation is well in line with the one made in determining the best substrate for block copolymer assembly (section 6.1). Even with the hydroxyl group producing treatments, the silicon wafers do not seem to have enough hydroxyl groups on the surface to bind MPTMS molecules. This must be due to the native oxide layer on the silicon wafer being weaker than expected. On the other hand, silica covered substrates already have much more oxygen on the surface and this must be why the hydroxylation worked better when using these substrates. In the following experiments, silicon or glass with 30 nm thick SiO_2 layer was used as substrate.

A new stamp with dimensions detectable by FLM was fabricated to study the attachment of MPTMS with a patterned stamp. The master was created by e-beam lithography and the stamp was fabricated from the master. The master contains lines, squares and chessboard patterns in 2 and 4 µm widths as depicted in Figure 6.16.

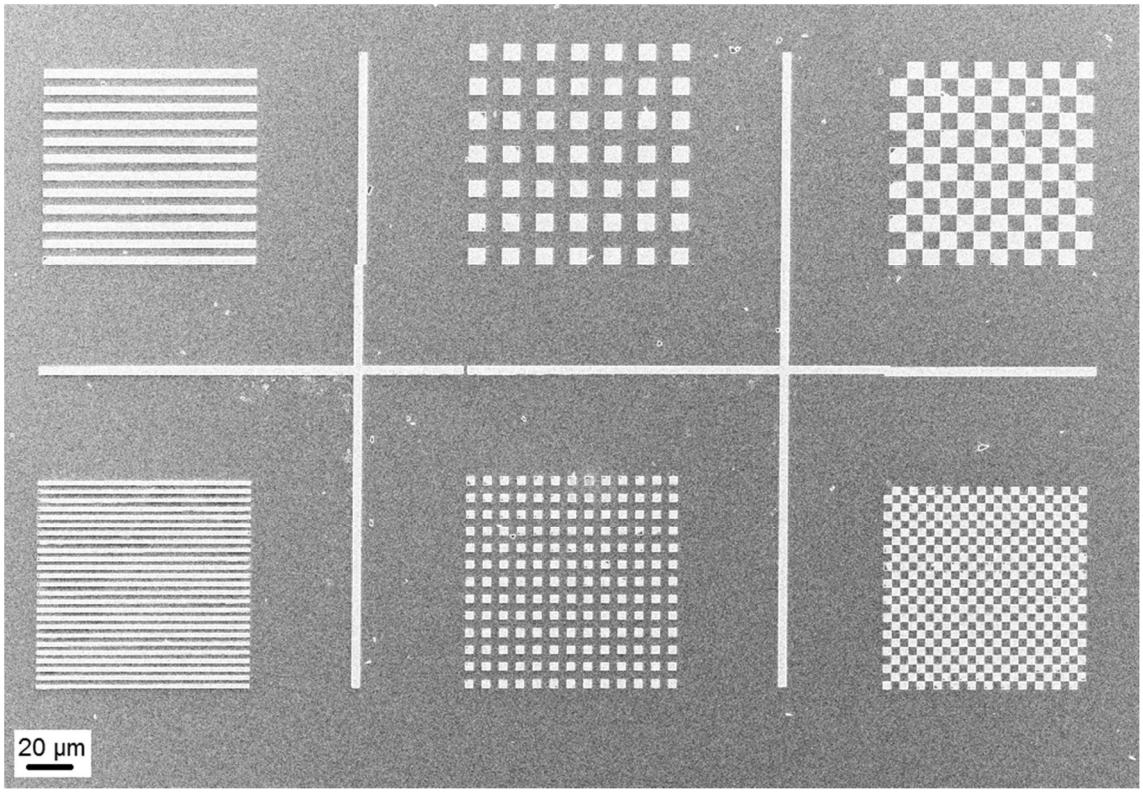

Figure 6.16. *SEM image of the master used for fabricating stamps for µCP process. The widths of the features in the upper row are 4µm and in the bottom row 2 µm.*

Microcontact printing process was then carried out with the newly fabricated stamp and MPTMS attachment was again studied with addition of mBBr fluorescent probe (Figure 6.17) and then the attachment of the colloidal quantum dots was attempted by dipping the MPTMS stamped substrate into 5 mM QD solution for 10 hours (Figure 6.18). Silicon and glass substrates with 30 nm SiO_2 layer were used.

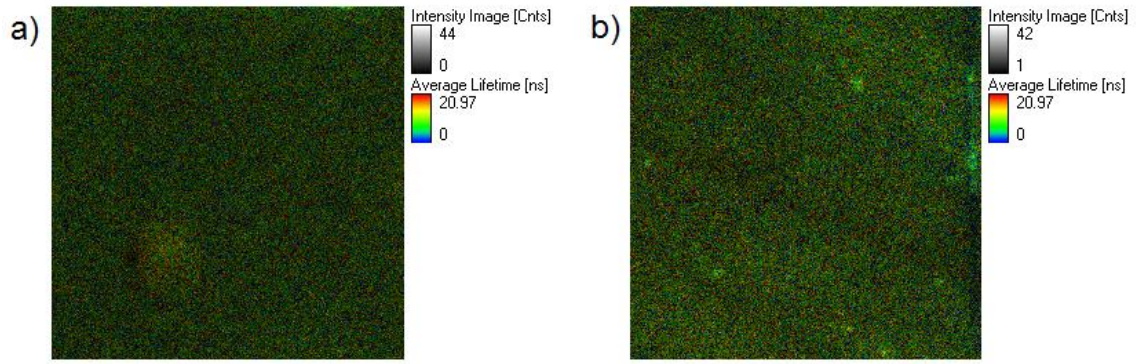

Figure 6.17. *FLM images of the results of a µCP process with MPTMS followed by a dip in mBBr fluorescent probe solution on a) silicon substrate with 30 nm SiO_2 layer on top and b) glass substrate with 30 nm SiO2 on top. The dimensions of each image are 40×40 µm.*

The stamping was directed with adjustment marks on the surface to facilitate locating the patterned area with FLM instrument and several FLM images were taken from that designated area inside the adjustment mark to make sure the whole stamped area was covered. In spite of these actions to ensure the patterned area was indeed being investigated, no stamped pattern was visible on either substrate. The FLM images were similar to the ones produced with flat stamps.

The reasons the stamp patterns are not visible in the FLM images are unknown. The pattern on the stamp should be ideal and the resolution of FLM instrument accurate enough to identify the 2 – 4 µm patterns. However, the effect of the contact time and pressure in microcontact printing should be studied more. It could be that the long contact time (500 s) causes diffusion of MPTMS molecules around the substrate surface, which prevents the formation of a self-assembled monolayer on specific locations determined by the features in the stamp. However, the conclusion to be drawn from the FLM images is that MPTMS layer must be present; otherwise there would not be any fluorescence from the mBBr because it is only fluorescent when attached to a thiol group. The reasons the stamped pattern cannot be seen have to be studied further.

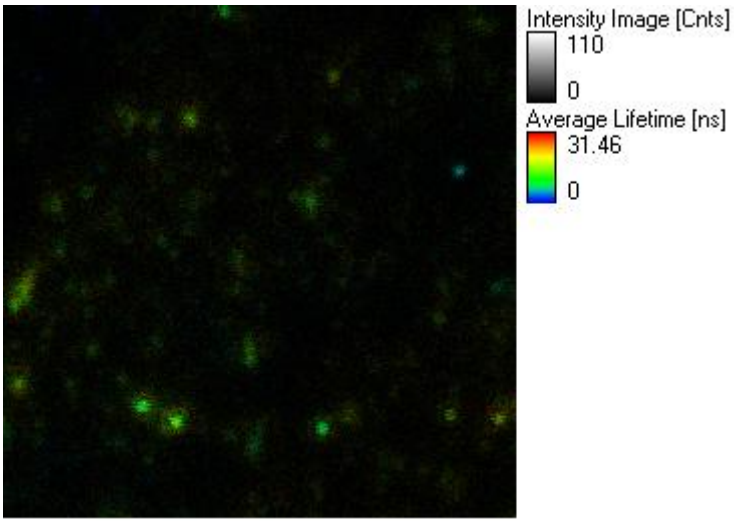

Figure 6.18. *FLM image of the results of a µCP process with MPTMS followed by a dip in quantum dot solution on a silicon substrate with 30 nm SiO_2 on top. The dimensions of the image are 40×40 µm.*

The FLM picture of the quantum dots on stamped MPTMS in Figure 6.16 points towards the notion that the stamping with MPTMS has not succeeded. The fluorescent emission of colloidal quantum dots is significantly weaker than that of thiol bound mBBr, which makes it more difficult to interpret the FLM images. Either way, there is no distinct pattern in the dimensions of the used stamp to be noticed, but the quantum dots are ordered on the surface quite randomly.

Stamping of MPTMS with a patterned stamp was also investigated by AFM and X-ray photoelectron spectroscopy (XPS) –measurements but neither of these showed any sign of patterns.

7 CONCLUSIONS

The underlying idea behind this Thesis is the prospect of taking advantage of the unique self-assembling properties of diblock copolymers and to use that to fabricate a stamp for microcontact printing and thus, achieve a nanoscale pattern of a self-assembling monolayer of (3-Mercaptopropyl)trimethoxysilane (MPTMS) on top of a substrate. This monolayer could then be further utilized to site controlled attachment of nanoparticles on a substrate surface.

The block copolymer lithography process for cylinder forming polystyrene-*block*-polymethyl metacrylate (PS-*b*-PMMA) block copolymers on both unpatterned and patterned surfaces was established during the work for this Thesis. It was noted that the surface perpendicular alignment of the cylinders was improved if the silicon substrates were covered with a thin layer of SiO_2. This result implies that the native oxide layer on the silicon substrates is not sufficient to produce enough silanol groups, required for the grafting of the surface neutralizing underlayer, on the surface of the substrate. Masters for elastomeric stamp fabrication were prepared from the assembled block copolymer templates and the comparison of different dry etching parameters revealed that CHF_3/O_2 etching produces the best overall results. However, the stamp fabrication process and the testing of the stamps with a NIL process pointed out that even in the best masters, the patterns are not deep enough to produce a usable stamp for microcontact printing. Thus, the etching parameters and the stamp fabrication materials and processes have to be reconsidered in the future studies. The microcontact printing process and the attachment of MPTMS molecules to the substrates was also investigated. Fluorescence lifetime microscopy measurements revealed that while the microcontact printing of MPTMS with a flat, unpatterned stamp worked well, the stamped patterns were not visible on the substrates stamped with a patterned stamp. The chemistry of MPTMS attachment has to be studied more closely as the recent studies conducted by surface science laboratory located also in Optoelectronics Research Centre showed that the hydroxylation of the methoxy groups in MPTMS, that is required for the attachment, only takes place under a certain pH and in specific solvents. It now has to be considered how to adapt this knowledge to improve the microcontact printing process. New experiments and maybe even new research methods should be contemplated.

Because block copolymer lithography is a completely new field of study in Optoelectronics Research Centre, much of the experiments in this Thesis were aimed at developing a reproducible process for obtaining nanohole patterns by self-assembly of PS-*b*-PMMA block copolymers and guiding the self-assembly by lithographically predefined structures. Now that the basic process scheme is established, the following ex-

periments should be directed towards optimizing the master fabrication and stamp preparation processes as well as studying the chemistry behind microcontact printing process more closely. Different underlying layers than SiO_2 could be considered to ease the etching of the BCP pattern into the substrate. For example, silicon nitride could be applied under a thin layer of SiO_2 and the etching of this layer could be studied in case it was more efficient than the etching of SiO_2 or silicon.

Besides this particular approach, block copolymer lithography could also be utilized for directed assembly of nanoparticles in several different ways. For example, a block copolymer template could act as a nanohole template and the particles could be inserted in the holes by an ink-jet (or similar) technique. Another option worth considering is to grow semiconductor nanoparticles such as quantum dots directly into nanohole patterns made by BCP lithography by molecular beam epitaxy (MBE). In any case, block copolymers are a new and interesting approach in making templates for directed assembly of nanoparticles. By adjusting the composition and molecular weights of the blocks, a number of different types and sizes of nanopatterns can be obtained which can furthermore be guided into desired patterns by prepatterning the underlying substrate. This flexibility that is particular to block copolymer lithography opens up countless opportunities, which is why block copolymer lithography is guaranteed to be a big part of nano- and microfabrication in the future.

REFERENCES

[1] Sanders, D. P. Advances in Patterning Materials for 193 nm Immersion Lithography. Chemical Reviews 110(2010)1, pp. 321–360.

[2] Li, H., Huck, W. T. S. Polymers in nanotechnology. Current Opinion in Solid State & Materials Science 6(2002)1, pp. 3–8.

[3] Bates, F. S., Fredrickson, G. H. Block Copolymers—Designer Soft Materials. 52(1999)2, p. 32.

[4] R. R. Li, R. R., Dapkus, P.D., Thompson, M. E., Jeong, W. G., Harrison, C., Chaikin, P. M., Register R. A, Adamson, D.H. Dense arrays of ordered GaAs nanostructures by selective area growth on substrates patterned by block copolymer lithography. Applied Physics. Letters 76(2000)13, p. 1689

[5] Cheng, J. Y., Ross, C. A., Chan, V. Z.-H., Thomas, E. L., Lammertink, R., G. H., Vancso, G. J. Formation of a Cobalt Magnetic Dot Array via Block Copolymer Lithography. Advanced Materials 13(2001)15, pp. 1174–1178

[6] Thurn-Albrecht, T., Schotter, J., Kästle, G. A., Emley, N., Shibauchi, T., Krusin-Elbaum, L., Guarini, K., Black, C. T., Tuominen, M. T., Russell, T. P. Ultrahigh-Density Nanowire Arrays Grown in Self-Assembled Diblock Copolymer Templates. Science, 290(2000)5499, pp. 2126–2129.

[7] Chan, V. Z.-H., Hoffman, J., Lee, V. Y., Iatrou, H., Avgeropoulos, A., Hadjichristidis, N., Miller, R. D., Thomas, E. L. Ordered Bicontinuous Nanoporous and Nanorelief Ceramic Films from Self Assembling Polymer Precursors. Science 286(1999)5445, pp. 1716–1719.

[8] Park, H. J., Kang, M.-G., Guo, L. J. Large Area High Density Sub-20 nm SiO_2 Nanostructures Fabricated by Block Copolymer Template for Nanoimprint Lithography. ACS Nano 3(2009)9, pp. 2601–2608.

[9] Xia Y., Whitesides, G. M. Soft Lithography. Angewandte Chemie International. Edition 37(1998)5, pp. 550–575.

[10] Menard E., Rogers, J. Stamping Techniques for Micro- and Nanofabrication. In: Bhushan, B. (ed.). Springer Handbook of Nanotechnology. 3rd ed. 2007. Springer Berlin Heidelberg. pp. 279–298.

[11] Viheriälä J., Niemi, T., Kontio, J. Pessa, M. Nanoimprint Lithography - Next Generation Nanopatterning Methods for Nanophotonics Fabrication. In: Young, K. (ed.). Recent Optical and Photonic Technologies. 2010. InTech. pp. 275-298.

[12] Cole T., Lusth, J. C. Quantum-dot cellular automata. Progress in Quantum Electronics. vol. 25(2001)4, pp. 165–189.

[13] Handbook of Industrial Chemistry: Organic Chemicals - Access Engineering from McGraw-Hill. [WWW]. [Accessed on 22.5.2014]. Available at: http://accessengineeringlibrary.com/browse/handbook-of-industrial-chemistry-organic-chemicals.

[14] Gupta, A. Polymer Chemistry. Meerut, IND: Global Media, 2010.

[15] Fimmtech inc. Polymers. [WWW]. [Accessed on 27.5.2014]. Available: http://injectionmoldingonline.com/Molding101/Polymers.aspx.

[16] Fried, J. R. Polymer science and technology. 2nd ed. Upper Saddle River, NJ 2003, Prentice Hall. 688 p.

[17] Stoykovich M. P., Nealey, P. F. Block copolymers and conventional lithography. Materials Today 9(2006)9, pp. 20–29.

[18] Bates F. S., Fredrickson, G. H. Block Copolymer Thermodynamics: Theory and Experiment. Annual Reviews of Physical. Chemistry. 41(1990)1, pp. 525–557.

[19] Flory, P. J. Thermodynamics of High Polymer Solutions. Journal of Chemical Physics. 10(2004)1, pp. 51–61.

[20] Huggins, M. L. Some Properties of Solutions of Long-chain Compounds. Journal of Physical Chemistry 46(1942)1, pp. 151–158.

[21] Huggins, M. L. Theory of Solutions of High Polymers. Journal of American Chemical Society, 64(1942)7, pp. 1712–1719.

[22] Segalman, R. A. Patterning with block copolymer thin films. Materials Science and Engineering: R: Reports 48(2005)6, pp. 191–226.

[23] Leibler, L. Theory of Microphase Separation in Block Copolymers. Macromolecules 13(1980)6, pp. 1602–1617.

[24] Matsen M. W., Schick, M. Stable and unstable phases of a diblock copolymer melt. Physical Review Letters 72(1994)16, pp. 2660–2663.

[25] Xu, T., Kim, H.-C., DeRouchey, J., Seney, C., Levesque, C., Martin, P., Stafford C. M., Russell, T. P. The influence of molecular weight on nanoporous polymer films. Polymer 42(2001)21,pp. 9091–9095.

[26] Russell, T. P., Coulon, G., Deline, V. R., Miller, D. C. Characteristics of the surface-induced orientation for symmetric diblock PS/PMMA copolymers. Macromolecules 22(1989)12, pp. 4600–4606.

[27] Green, P. F., Christensen, T. M., Russell, T. P. Ordering at diblock copolymer surfaces. Macromolecules 24(1991)1, pp. 252–255.

[28] Harrison, C. K. Block copolymer microdomains in thin films. ProQuest Dissertations and Theses, PhD Thesis. Princeton 1999. Princeton University. Publication Number AAI9927805. 273 p.

[29] Fasolka M. J., Mayes, A. M. "Block Copolymer Thin Films: Physics and Applications. Annual Review of Materials Research 31(2001)1, p. 323.

[30] Zvelindovsky A. V., Sevink, G. J. A. Orthogonal fields: A path to long-range three-dimensional order in block copolymers. Journal of Chemical Physics 23(2005)7, p. 074903

[31] Darling, S. B. Directing the self-assembly of block copolymers. Progress in Polymer Science 32(2007)10, pp. 1152–1204.

[32] Smith, A. P., Douglas, J. F., Meredith, J. C., Amis, E. J., Karim, A. Combinatorial Study of Surface Pattern Formation in Thin Block Copolymer Films. Physical Review Letters 87(2001)1, p. 015503.

[33] Mansky, P. Controlling Polymer-Surface Interactions with Random Copolymer Brushes. Science 275(1997)5305 pp. 1458–1460.

[34] Peters, R. D., Nealey, P. F., Crain, J. N., Himpsel, F. J. A Near Edge X-ray Absorption Fine Structure Spectroscopy Investigation of the Structure of Self-Assembled Films of Octadecyltrichlorosilane. Langmuir 18(2002)4, pp. 1250–1256.

[35] Peters, R. D. Yang, X. M., Kim, T. K., Sohn, B. H., Nealey, P. F. Using Self-Assembled Monolayers Exposed to X-rays To Control the Wetting Behavior of Thin Films of Diblock Copolymers. Langmuir 16(2000)10, pp. 4625–4631.

[36] Ryu, D. Y., Shin, K., Drockenmuller, E., Hawker, C. J., Russell, T. P. A Generalized Approach to the Modification of Solid Surfaces. Science 308(2005)5719, pp. 236–239.

[37] Ji, S., Liu, G., Zheng, F., Craig, G. S. W., Himpsel, F. J., Nealey, P. F. Preparation of Neutral Wetting Brushes for Block Copolymer Films from Homopolymer Blends. Advanced Materials 20(2008)16, pp. 3054–3060.

[38] Amundson, K., Helfand, E., Quan, X., Hudson, S. D., Smith, S. D. Alignment of Lamellar Block Copolymer Microstructure in an Electric Field. 2. Mechanisms of Alignment. Macromolecules 27(1994)22, pp. 6559–6570.

[39] Morkved, T. L., Lu, M., Urbas, A. M., Ehrichs, E. E., Jaeger, H. M., Mansky, P., Russell, T. P. Local Control of Microdomain Orientation in Diblock Copolymer Thin Films with Electric Fields. Science 273(1996)5277, pp. 931–933.

[40] Mansky, P., DeRouchey, J., Russell, T. P., Mays, J., Pitsikalis, M., Morkved, T., Jaeger, H. Large-Area Domain Alignment in Block Copolymer Thin Films Using Electric Fields, Macromolecules 31(1998)13, pp. 4399–4401.

[41] Grigorova, T., Pispas, S., Hadjichristidis, N., Thurn-Albrecht, T. Magnetic Field Induced Orientation in Diblock Copolymers with One Crystallizable Block. Macromolecules 38(2005)17, pp. 7430–7433.

[42] Kim, S. H., Misner, M. J., Russell, T. P. Solvent-Induced Ordering in Thin Film Diblock Copolymer/Homopolymer Mixtures. Advanced Materials 16(2004)23-24, pp. 2119–2123.

[43] Ouk Kim, S., Solak, H. H., Stoykovich, M. P., Ferrier, N. J., de Pablo, J.J.,. Nealey, P. F. Epitaxial self-assembly of block copolymers on lithographically defined nanopatterned substrates. Nature 424(2003)6947, pp. 411–414.

[44] Park, S.-M., Craig, G. S. W., La, Y.-H., Solak, H. H., Nealey, P. F. Square Arrays of Vertical Cylinders of PS-b-PMMA on Chemically Nanopatterned Surfaces. Macromolecules 40(2007)14, pp. 5084–5094.

[45] Bao, X.-Y., Yi, H., Bencher, C., Chang, L.-W., Dai, H., Chen, Y., Chen, P.-T. J., Wong H.-S. P., SRAM, NAND, DRAM contact hole patterning using block copolymer directed self-assembly guided by small topographical templates. Electron Devices Meeting (IEDM), 2011 IEEE International, 2011, pp. 7.7.1–7.7.4.

[46] Kim, H.-C., Park, S.-M., Hinsberg, W. D. Block Copolymer Based Nanostructures: Materials, Processes, and Applications to Electronics. Chemical Reviews 110(2010)1, pp. 146–177.

[47] Hamley, I. W. Ordering in thin films of block copolymers: Fundamentals to potential applications. Progress in Polymer Science 34(2009)11, pp. 1161–1210.

[48] Smith H. I., Flanders, D. C. Oriented crystal growth on amorphous substrates using artificial surface-relief gratings. Applied Physics Letters 32(1978)6, pp. 349–350.

[49] Segalman, R. A., Yokoyama, H., Kramer, E. J. Graphoepitaxy of Spherical Domain Block Copolymer Films. Advanced Materials 13(2001)15, pp. 1152–1155.

[50] Jung, Y. S., Jung, W., Ross, C. A. Nanofabricated Concentric Ring Structures by Templated Self-Assembly of a Diblock Copolymer. Nano Letters 8(2008)9, pp. 2975–2981.

[51] Cheng, J. Y., Ross, C. A., Thomas, E. L., Smith, H. I., Vancso, G. J. Fabrication of nanostructures with long-range order using block copolymer lithography. Applied Physics Letters 81(2002)19, p. 3657.

[52] Sundrani, D., Darling, S. B., Sibener, S. J. Guiding Polymers to Perfection: Macroscopic Alignment of Nanoscale Domains. Nano Letters 4(2004)2, pp. 273–276.

[53] Ruiz, R., Ruiz, N., Zhang, Y., Sandstrom, R. L., Black, C. T. Local Defectivity Control of 2D Self-Assembled Block Copolymer Patterns. Advanced Materials 19(2007)16, pp. 2157–2162.

[54] Park, S.-M., Stoykovich, M. P., Ruiz, R.,Zhang, Y., Black, C. T., Nealey, P. F. Directed Assembly of Lamellae- Forming Block Copolymers by Using Chemically and Topographically Patterned Substrates. Advanced Materials 19(2007)4, pp. 607–611.

[55] Sundrani, D., Darling, S. B., Sibener, S. J. Hierarchical Assembly and Compliance of Aligned Nanoscale Polymer Cylinders in Confinement. Langmuir 20(2004)12, pp. 5091–5099.

[56] Black C. T., Bezencenet, O. Nanometer-scale pattern registration and alignment by directed diblock copolymer self-assembly. IEEE Transactions on Nanotechnology 3(2004)3, pp. 412–415.

[57] Luo M., Epps, T. H. Directed Block Copolymer Thin Film Self-Assembly: Emerging Trends in Nanopattern Fabrication. Macromolecules 46(2013)19, pp.7567-7579

[58] Yang, X., Wan, L., Xiao, S., Xu, Y., Weller, D. K. Directed Block Copolymer Assembly versus Electron Beam Lithography for Bit-Patterned Media with Areal Density of 1 Terabit/inch2 and Beyond, ACS Nano 3(2009)7, pp. 1844–1858.

[59] Edwards, E. W., Montague, M. F., Solak, H. H., Hawker, C. J., Nealey, P. F. Precise Control over Molecular Dimensions of Block-Copolymer Domains Using the Interfacial Energy of Chemically Nanopatterned Substrates. Advanced Materials 16(2004)15, pp. 1315–1319.

[60] Park, S. H., Shin, D. O., Kim, B. H., Yoon, D. K., Kim, K., Lee, S. Y., Oh, S.-H., Choi, S.-W., Jeon, S. C., Kim, S. O. Block copolymer multiple patterning integrated with conventional ArF lithography. Soft Matter 6(2010)1, p. 120.

[61] Stoykovich, M. P., Kang, H., Daoulas, K. C., Liu, G., Liu, C.-C., de Pablo, J. J., Müller, M., Nealey, P. F. Directed Self-Assembly of Block Copolymers for Nanolithography: Fabrication of Isolated Features and Essential Integrated Circuit Geometries. ACS Nano 1(2007)3, pp. 168–175.

[62] Ruiz, R., Kang, H., Detcheverry, F. A., Dobisz, E., Kercher, D. S., Albrecht, T. R., de Pablo, J. J., Nealey, P. F. Density Multiplication and Improved Lithography by Directed Block Copolymer Assembly. Science 321(2008)5891, pp. 936–939.

[63] Welander, A. M., Kang, H., Stuen, K. O., Solak, H. H., Müller, M., de Pablo, J. J., Nealey, P. F. Rapid Directed Assembly of Block Copolymer Films at Elevated Temperatures. Macromolecules 41(2008)8, pp. 2759–2761.

[64] Mack, C. Fundamental Principles of Optical Lithography : The Science of Microfabrication. Hoboken, NJ, USA 2008, Wiley. 534 p.

[65] Franssila, S. Introduction to Microfabrication. (2nd ed.). Hoboken, NJ, USA 2010, Wiley. 534 p.

[66] Rai-Choudhury, P. (ed). Handbook of microlithography, micromachining, and microfabrication. Bellingham, Washington, USA 1997, Institution of Electrical Engineers. 692 p.

[67] Grenon, B. J. Electron-Beam Lithography. In: Wiley Encyclopedia of Electrical and Electronics Engineering. John Wiley & Sons, Inc., 2001.

[68] Vieu, C., Carcenac, F., Pépin, A., Chen, Y., Mejias, M., Lebib, A., Manin-Ferlazzo, L., Couraud, L., Launois, H. Electron beam lithography: resolution limits and applications. Applied Surface Science 164(2000)1-4, pp. 111–117.

[69] Kumar A., Whitesides, G. M. Features of gold having micrometer to centimeter dimensions can be formed through a combination of stamping with an elastomeric stamp and an alkanethiol "ink" followed by chemical etching. Applied Physics Letters 63(1993)14, pp. 2002–2004.

[70] Xia, Y., Kim, E., Zhao, X.-M., Rogers, J. A., Prentiss, M., Whitesides, G. M. Complex Optical Surfaces Formed by Replica Molding Against Elastomeric Masters. Science 273(1996)5273, pp. 347–349.

[71] Zhao, X.-M., Xia, Y., Whitesides, G. M. Fabrication of three-dimensional micro-structures: Microtransfer molding. Advanced Materials 8(1996)10, pp. 837–840.

[72] Loo, Y.-L., Willett, R. L., Baldwin, K. W., Rogers, J. A. Interfacial Chemistries for Nanoscale Transfer Printing Journal of American Chemical Society 124(2002)26, pp. 7654–7655.

[73] Chou, S. Y., Krauss, P. R., Renstrom, P. J. Imprint of sub-25 nm vias and trenches in polymers. Applied Physics Letter 67(1995)21, pp. 3114–3116.

[74] Delamarche, E., Schmid, H., Michel, B., Biebuyck, H. Stability of molded polydimethylsiloxane microstructures, Advanced Materials 9(1997)9, pp. 741–746.

[75] Wood V., Bulovic, V. Colloidal quantum dot light-emitting devices. Nano Reviews 1(2010), Jul. 2010.

[76] Shirasaki, Y., Supran, G. J., Bawendi, M. G., Bulović, V. Emergence of colloidal quantum-dot light-emitting technologies. Nature Photonics 7(2013)1, pp. 13–23.

[77] Talapin, D. V., Rogach, A. L., Kornowski, A., Haase, M., Weller, H. Highly Luminescent Monodisperse CdSe and CdSe/ZnS Nanocrystals Synthesized in a Hexadecylamine−Trioctylphosphine Oxide−Trioctylphospine Mixture. Nano Letters 1(2001)4, pp. 207–211.

[78] Radhakrishnan, C., Lo, M. K. F., Knobler, C. M., Garcia-Garibay, M. A., Monbouquette, H. G. Capping-Ligand Effect on the Stability of CdSe Quantum Dot Langmuir Monolayers. Langmuir 27(2011)6, pp. 2099–2103.

[79] Shen Y.-J., Lee, Y.-L. Assembly of CdS quantum dots onto mesoscopic TiO2 films for quantum dot-sensitized solar cell applications. Nanotechnology 19(2008)4, p. 045602.

[80] Robel, I., Subramanian, V., Kuno, M., Kamat, P. V. Quantum Dot Solar Cells. Harvesting Light Energy with CdSe Nanocrystals Molecularly Linked to Mesoscopic TiO2 Films. Journal of the. American Chemical Society 128(2006)7, pp. 2385–2393.

[81] V. L. Colvin, M. C. Schlamp, and A. P. Alivisatos, “Light-emitting diodes made from cadmium selenide nanocrystals and a semiconducting polymer,” *Nature*, vol. 370, no. 6488, pp. 354–357, Aug. 1994.

[82] Pattantyus-Abraham, A. G., Kramer, I. J., Barkhouse, A. R., Wang, X., Konstanatos, G., Debnath, R., Levina, L., Raabe, I., Nazeeruddin, M. K., Grätzel, M., Sargent, E. H. Depleted-Heterojunction Colloidal Quantum Dot Solar Cells. ACS Nano 4(2010)6, pp. 3374–3380.

[83] Pal, B. N., Robel, I., Mohite, A., Laocharoensuk, R., Werder, D. J., Klimov, V. I. High-Sensitivity p–n Junction Photodiodes Based on PbS Nanocrystal Quantum Dots. Advanced Functional Materials 22(2012)8, pp. 1741–1748.

[84] Medintz, I. L., Uyeda, H. T., Goldman, E. R., Mattoussi, H. Quantum dot bioconjugates for imaging, labelling and sensing. Nature Materials 4(2005)6, pp. 435–446.

[85] Thurn-Albrecht, T., Steiner, R., DeRouchey, J., Stafford, C. M., Huang, E., Bal, M., Tuominen, M., Hawker, C. J., Russell, T. P. Nanoscopic Templates from Oriented Block Copolymer Films. Advanced Materials 12(2000)11, pp. 787–791.

[86] In, I., La, Y.-H., Park, S.-M., Nealey, P. F., Gopalan, P. Side-Chain-Grafted Random Copolymer Brushes as Neutral Surfaces for Controlling the Orientation of Block Copolymer Microdomains in Thin Films. Langmuir 22(2006)18, pp. 7855–7860.

[87] Allresisit GmbH. Positive PMMA E-Beam Resists AR-P 630-670 series. [WWW]. [Accessed on 11.07.2014]. Available: http://www.allresist.com/wp-content/uploads/sites/2/2014/02/allresist_produktinfos_ar-p630-690_englisch.pdf

[88] Micro Resist Technology GmbH. UV-curable polymers for UV-based nanoimprint lithography. [WWW] [Accessed on 11.07.2014] Available: http://www.microchem.com/PDFs_MRT/mr-UVCur%2021%20+%20mr-UVCur06%20Overview.pdf

[89] Schmid H., Michel, B. Siloxane Polymers for High-Resolution, High-Accuracy Soft Lithography. Macromolecules 33(2000)8, pp. 3042–3049.

[90] Beck, M., Graczyk, M., Maximov, I., Sarwe, E.-L., Ling, T. G. I., Keil, M., Montelius, L. Improving stamps for 10 nm level wafer scale nanoimprint lithography. Microelectronics Engineering 61–62(2002), pp. 441–448.

[91] Viheriälä, J., Tommila, J., Leinonen, T., Dumitrescu, M., Toikkanen, L.,. Niemi, T., Pessa, M. Applications of UV-nanoimprint soft stamps in fabrication of single-frequency diode lasers. Microelectronics Engineering 86(2009)3, pp. 321–324.

[92] Ulman, A. Formation and Structure of Self-Assembled Monolayers. Chemical Reviews 96(1996)4, pp. 1533–1554.

[93] Libioulle, L., Bietsch, A., Schmid, H., Michel, B., Delamarche, E. Contact-Inking Stamps for Microcontact Printing of Alkanethiols on Gold. Langmuir 15(1999)2, pp. 300–304.

[94] Purdue University. Scanning Electron Microscope. [WWW]. [Accessed on 24.06.2014]. Available: https://www.purdue.edu/ehps/rem/rs/sem.htm.

[95] ASM International, *ASM handbook*, 10th ed. Materials Park, OH 1990. ASM International.

[96] Bowen W. R., Hilal, N. Atomic force microscopy in process engineering introduction to AFM for improved processes and products. Oxford; Burlington, MA 2009. Butterworth-Heinemann.

[97] Eaton, P. J. Atomic force microscopy. Oxford ; New York 2010. Oxford University Press.

[98] Lehtivuori, H. Photodynamics of Energy and Electron Transfers in Solid Films of Porphyrin, Phthalocyanine, and Perylene Diimide Derivatives. Dissertation, Tampere University of Technology, Tampere, 2010.

[99] Chinn, P. C., Pigiet, V., Fahey, R. C. Determination of thiol proteins using monobromobimane labeling and high-performance liquid chromatographic analysis: Application to Escherichia coli thioredoxin. Analytical Biochemistry. 159(1986)1, pp. 143–149.

APPENDIX 1: BLOCK COPOLYMER LITHOGRAPHY – BASIC PROCESS

Material: Silicon wafer
10nm SiO_2 growth.
10 min Piranha treatment (H_2SO_4:H_2O_2 4:1)
O_2 plasma activation
PS-r-PMMA 2 wt% spin coat 1500rpm, 30s
Anneal in reflow oven 175°C 72h
Toluene spin wash x3
PS-b-PMMA (1wt% in toluene) spin coat 3000-3500rpm. 30s
Anneal in reflow oven 185°C 48h
PMMA domain etch off: RIE O_2/Ar 15:3sccm, 12mTorr, 20W, 26s)

APPENDIX 2: TOPOGRAPHICAL PATTERNING PROCESS

Material: Silicon wafer
Clean with acetone + methanol
PMMA photoresist (ARP 672.03) spin coat 2000rpm, closed lid. (~110nm thick)
Bake at 170°C for 2 min
E-beam patterning of the desired pattern (lattices). Aperture size 20 nm, electron beam current 10 kV.
Resist development MIBK:IPA (1:3) 30s + IPA rinse 30s
Si etch with RIE: SF_6/O_2 30/3sccm, 30mTorr, 175W, 7s (63nm)
PMMA removal with sonication in toluene, 20 min 40°C
10 – 30 nm SiO_2 growth with PECVD
10 min Piranha treatment (H_2SO_4:H_2O_2 4:1)
O_2 activation
PS-*r*-PMMA (2 wt% in toluene) spin coat 1500rpm, 30s
Anneal in reflow oven 175°C 72h
Toluene spin wash x3
PS-*b*-PMMA (1wt% in toluene) spin coat 3000 - 3500rpm. 30s
Anneal in reflow oven 185°C 48h
PMMA domain etch off: RIE O_2/Ar 15:3sccm, 12mTorr, 20W, 26s)

APPENDIX 3: TOPOGRAPHICAL PATTERNING PROCESS WITH GOLD SIDEWALLS

Material: Silicon wafer
10 – 30 nm SiO_2 growth.
10 min Piranha treatment (H_2SO_4:H_2O_2 4:1)
O_2 plasma activation
PS-*r*-PMMA (2 wt% in toluene) spin coat 1500rpm, 30s
Anneal in reflow oven 175°C 72h
Toluene spin wash x3
PMMA photoresist (ARP 672.03) spin coat 2000rpm, closed lid. (~110nm thick)
Bake at 170°C for 2 min
E-beam patterning of the desired pattern (lattices). Aperture size 20 nm, electron beam current 10 kV.
Resist development MIBK:IPA (1:3) 50s + IPA rinse 30s
5nm Cr + 40nm / 50nm Au evaporation with e-beam evaporator
Liftoff with sonication in toluene, 20min 40°C
Check the pattern quality with SEM
PS-*b*-PMMA (1wt% in toluene) spin coat 3000 - 3500rpm, 30s
Anneal in reflow oven 185°C 48h
PMMA domain etch off: RIE O_2/Ar 15:3sccm, 12mTorr, 20W, 26s)